Multiple band structures of ^{131}Cs

S. Sihotra,[1,2,3] R. Palit,[2,*] Z. Naik,[2] K. Singh,[1] P. K. Joshi,[2] A. Y. Deo,[2] J. Goswamy,[1] S. S. Malik,[3] D. Mehta,[1] C. R. Praharaj,[4] H. C. Jain,[2] and N. Singh[1]

[1]*Department of Physics, Panjab University, Chandigarh-160014, India*

[2]*Department of Nuclear and Atomic Physics, Tata Institute of Fundamental Research, Mumbai-400005, India*

[3]*Department of Physics, Guru Nanak Dev University, Amritsar-143005, India*

[4]*Institute of Physics, Bhubaneswar-751005, India*

(Received 7 January 2008; revised manuscript received 13 June 2008; published 22 September 2008)

Excited states in ^{131}Cs were investigated through in-beam γ-ray spectroscopic techniques following its population in the ^{124}Sn(^{11}B, $4n$) fusion-evaporation reaction at a beam energy of 46 MeV. The previously known level scheme has been substantially extended up to ~9 MeV excitation energy and $49/2\hbar$ spin with the addition of seven new band structures. The present level scheme consisting of 15 bands exhibits a variety of collective features in this nucleus at intermediate spin. The excitation energies of the observed levels in different bands and the corresponding ratios of transition strengths, i.e., $B(M1)/B(E2)$, have been compared with the results of projected deformed Hartree-Fock calculations based on various quasiparticle configurations. A strongly coupled band has been reassigned a high-K three-quasiparticle $\pi h_{11/2} \otimes \nu(h_{11/2}d_{3/2})$ configuration based on the properties of this band and that of its new coupled side band. The configurations of these bands are also discussed in the framework of tilted-axis cranking model calculations and the systematics of the odd-A Cs isotopes. Additional three energetically closely placed coupled bands have been assigned different unpaired three-quasiparticle configurations. γ-vibrational bands coupled to the $\pi h_{11/2}$ and $\pi g_{7/2}$ single-particle configurations have been reported in this nucleus. Observation of new $E1$ transitions linking the opposite-parity $\pi h_{11/2}$ and $\pi d_{5/2}$ bands provides fingerprints of possible octupole correlations.

DOI: 10.1103/PhysRevC.78.034313 PACS number(s): 21.10.Hw, 21.60.−n, 23.20.En, 27.60.+j

I. INTRODUCTION

The nuclei in the $A \sim 130$ mass region below the $N = 82$ shell closure are soft to γ deformation at low and medium spins, and exhibit various intriguing phenomena [1–3]. For these nuclei, the proton Fermi surface lies low within the $h_{11/2}$ orbitals driving the nucleus to prolate shape, whereas the neutron Fermi surface lies near the middle of the $h_{11/2}$ orbitals favoring an oblate shape [4]. Because of the opposite types of quadrupole deformations for the proton and neutron mass distributions, these nuclei develop γ instability and provide an opportunity to investigate the evolution of collectivity and the competing nuclear shapes with increasing spin and as a function of positions of neutron and proton Fermi surfaces in the unique-parity $h_{11/2}$ intruder orbital. The γ-soft behavior of the $A \sim 130$ even-even nuclei is manifested by the energy staggering observed in the quasi-γ bands [5]. For the odd-Z nuclei, the level structure at low spin is mainly influenced by the valance quasiproton coupled with the even-even core. At higher frequencies, shape changes have been found to occur, in particular, due to additional rotationally aligned quasiparticles polarizing the γ-soft core depending upon the position of the Fermi surfaces [6,7]. Depending upon the coupling of angular momenta of the valence neutrons and protons with that of the even-even core, different types of excitations, namely, magnetic rotation, chiral twin bands, and recently predicted chopstick configurations, have been discussed for this mass region [8–14]. The appearance of $\Delta I = 1$ bands characterized by rapidly decreasing $B(M1)$ strength with increasing spin have been interpreted in terms of coupling of angular momenta of proton particles (holes) and neutron holes (particles) in high j orbitals in a moderately deformed core. On the other hand, the twin degenerate dipole bands with similar energy staggering and electromagnetic strengths were explained with aplanar tilted rotation of the triaxial core along with the valence neutrons and protons aligned along the two extreme axes of the core. The truncated shell model calculation prescribes another angular momentum coupling scheme, namely, the chopstick model, which predicts a series of degenerate dipole band structures in nuclei around the $A \sim 130$ region. Extensive studies have been carried out using the Woods-Saxon-based cranking model to investigate the ground state shapes and quasiparticle alignments for even-even nuclei in this region [15]. Systematic studies on these nuclei in the $A \sim 130$ region have also been carried out based on algebraic models to describe the low-lying states and thereby probing the underlying symmetries [16–18]. The triaxial rotor plus particle model has been used to explain the negative-parity states in the ^{125,127,129}Cs isotopes [19]. The odd-even nuclei provide the possibility of studying different types of coupling of the valence proton with the even-even core and its excitations. The presence of nearby $h_{11/2}$, $g_{7/2}$, and $d_{5/2}$ proton orbitals usually gives rise to different one-quasiparticle band structures, and further rearrangements of neutrons and protons add richness to the structure. As the $h_{11/2}$ and $d_{5/2}$ orbitals with $\Delta l = 3$ are near the Fermi surface, octupole collectivity will be enhanced in this region and has been observed in Cs isotopes like ^{122}Cs [20] and ^{141,143}Cs [21] and also in the neighboring Xe and Ba isotopes. The low-lying states in ^{131}Cs

*Corresponding author: palit@tifr.res.in

have been found to be previously established through the electron-capture decay of ^{131}Ba [22]. High spin states of ^{131}Cs have been reported by Garg *et al.* [23] using the ^{124}Sn(^{10}B, $3n$) and ^{128}Te(^{6}Li, $3n$) reactions. Recently, collective structures of the ^{131}Cs nucleus have been reported by Kumar *et al.* [24], who observed a number of multiquasiparticle bands based on different configurations.

In this work, we report on new results of a detailed study of the level structure of ^{131}Cs. The developed level scheme shows interesting band structures involving degenerate $\Delta I = 1$ doublet bands, quasivibrational structures, and signatures of octupole collectivity. The experimental details and results of the present measurements are described in Secs. II and III. Deformed Hartree-Fock and the tilted-axis cranking calculations are performed for ^{131}Cs in the present work. The calculation procedures are outlined in Sec. IV. The structures of most of the bands are interpreted in Sec. V, based on comparison with theoretical results and the systematics of neighboring nuclei. The configurations of the nearly degenerate dipole bands were compared with calculations based on multiquasiparticle configurations with different K values. At the end, the quasivibrational bands and the relative strengths of $E1$ transitions are discussed only with the available systematics of the neighboring nuclei.

II. EXPERIMENTAL DETAILS AND DATA ANALYSIS

Excited states of the ^{131}Cs nucleus were populated in our experiment through the ^{124}Sn(^{11}B, $4n$)^{131}Cs fusion-evaporation reaction using a 46 MeV ^{11}B beam from the 14-UD Pelletron at the Bhabha Atomic Research Centre (BARC)-Tata Institute of Fundamental Research (TIFR) in Mumbai, India. The target consisted of isotopically enriched ^{124}Sn foil of thickness 1.6 mg/cm^2 rolled onto a 12.6 mg/cm^2 thick Au backing. The experimental setup consisted of eight Compton-suppressed clover detectors placed in the horizontal plane at 60°, 90°, 120°, 150°, 210°, 250°, 285°, and 325° with respect to the beam direction. The photopeak efficiency of this clover array was ∼1.6% for the 1.3 MeV γ rays. A 14-element NaI(Tl) multiplicity filter [13] in the form of two clusters was also placed above and below the horizontal plane. Each of the clover detectors was treated as a single detector. The master trigger for collecting γ-γ coincidence data was generated with the condition that at least two clover detectors and two NaI(Tl) detectors fired in coincidence. The clover detectors were calibrated for γ-ray energies and efficiencies using the ^{133}Ba and ^{152}Eu radioactive sources. The collected γ-γ coincidence data were sorted into a two-dimensional matrix. The background from this γ-γ matrix was subtracted using the method outlined in Ref. [25]. The background-subtracted matrix has around 150×10^6 coincidences. From the γ-γ coincidence data, the intensity, directional correlation of oriented states (DCO) ratio, and polarization asymmetry of different transitions were extracted and used for establishing the level scheme of ^{131}Cs. The partial level scheme of ^{131}Cs developed in the present work is shown in Figs. 1 and 2.

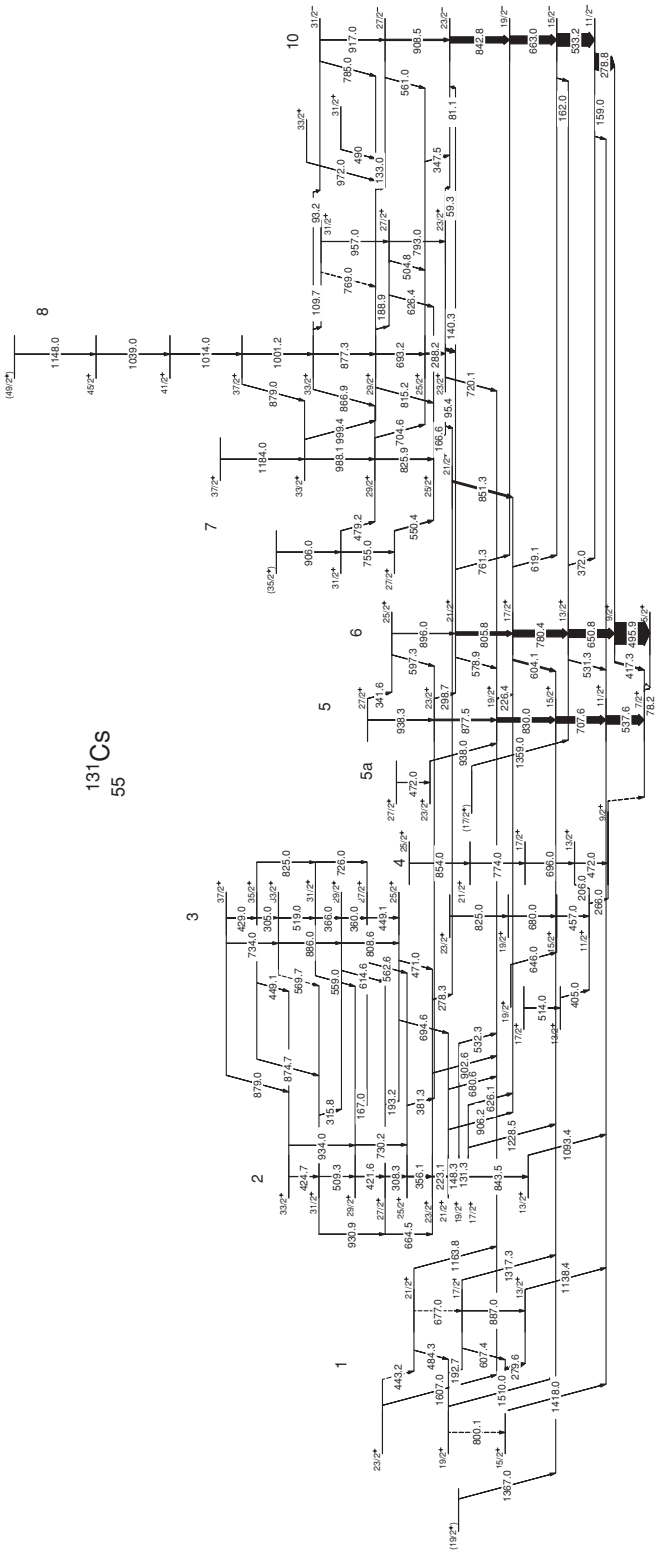

FIG. 1. Partial level scheme of ^{131}Cs (part I.).

Relative intensities of γ rays in ^{131}Cs were extracted from single-γ spectra and γ-γ coincidence spectra. Intensity for each γ-ray was obtained from the peak area corrected for efficiencies of the clover detectors. Intensities have been normalized with respect to the 495.9 keV ($\frac{9}{2}^+ \rightarrow \frac{5}{2}^+$) transition.

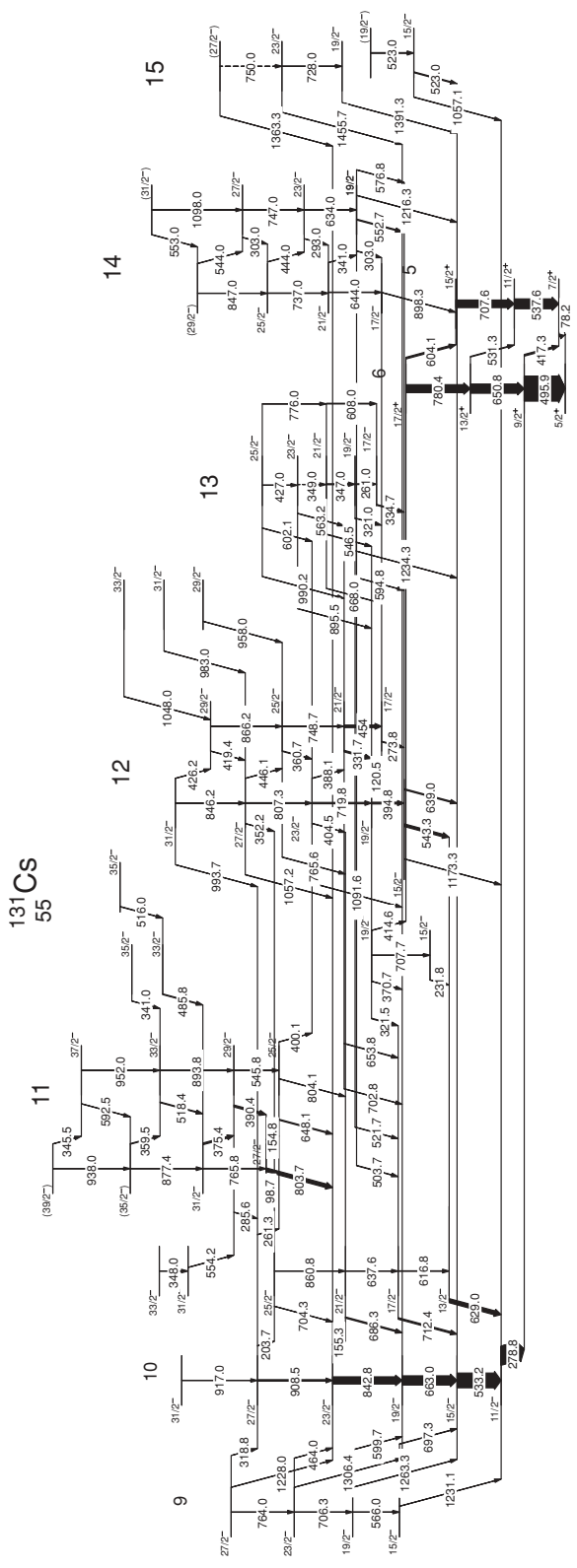

FIG. 2. Partial level scheme of ^{131}Cs (part II.).

The intensities of the weaker transitions were obtained from the added spectra with gates on various γ-ray transitions. The intensities of the γ rays obtained from the coincidence spectra were normalized to those obtained from single-γ spectra. The relative intensities of various transitions obtained in the present work are listed in Table I.

The multipolarity of different transitions has been determined from an angular correlation analysis using the method of directional correlation from oriented states (DCO) [26]. The coincidence events were sorted into an asymmetric matrix with the 30° detectors on one axis and 90° detectors on the other axis. By setting gates on the transition with known multipolarity (either pure quadrupole or dipole) along the two axes of this matrix, the peak areas $A_{\gamma p}(30^{\circ})$ and $A_{\gamma p}(90^{\circ})$ were obtained from the projected spectra and were further used to deduce the DCO ratios. For most of the transitions, DCO ratios were obtained from the gate on the 495.9 keV ($9/2^+ \rightarrow 5/2^+$), 537.6 keV ($11/2^+ \rightarrow 7/2^+$), and 533.2 keV ($15/2^- \rightarrow 11/2^-$) $E2$ transitions. For the weaker transitions, the DCO ratios were obtained from the added spectra with the gate on the quadrupole transitions. The DCO ratios extracted in this geometry are typically $\geqslant 1.0$ for quadrupole transitions and $\leqslant 0.6$ for dipole transitions. The DCO values for different γ-ray transitions are given in Table I.

Clover detectors have been used as polarimeters to measure the polarization [27,28] of γ rays to determine the electric or magnetic character of transitions. We have performed integrated polarization asymmetry measurements (IPDCO) by taking all the detectors into consideration [13,27]. The values of the polarization asymmetry obtained from these measurements are listed in Table I.

III. RESULTS

The present level scheme of ^{131}Cs, shown in Figs. 1 and 2, is built on the ground state ($T_{1/2} = 9.688$ d) with $I^{\pi} = 5/2^+$ and consists of around 15 bands. The positive-parity bands have been labeled B1–B8, and the negative-parity bands have been labeled B9–B15 to facilitate the discussion. The level scheme from the present work is established up to 9 MeV excitation energy and $49/2\hbar$ spin and is a significant extension with the addition of about 260 new transitions to those reported in the earlier works by Garg *et al.* [23] and more recently by Kumar *et al.* [24]. The present level scheme preserves major features of the previously observed bands B5, B6, and B10, which have been assigned to be based on the $\pi g_{7/2}$, $\pi d_{5/2}$, and $\pi h_{11/2}$ orbitals, respectively. Seven bands, namely, B1, B3, B4, B9, B13, B14, and B15, have been reported for the first time. In addition, several new intraband and interband transitions have been placed. The coincidence spectra with gates on various γ lines, which show the new transitions, are depicted in Figs. 3–5. The spins and parities of the different band structures were assigned on the basis of the results of angular correlation and polarization measurements. Higher excited positive-parity bands have been found to decay into the different levels of positive parity $\pi g_{7/2}$ (B5) and $\pi d_{5/2}$ (B6) bands and most of the higher excited negative-parity bands decay into different levels of band B10 based on $\pi h_{11/2}$ orbital, which in turn also decays to different levels of B5 and B6 bands. Details of the bands B1–B15 of ^{131}Cs as obtained in the present work are discussed below.

TABLE I. Relative intensities, DCO, and PDCO ratios for γ transitions of energy E_γ, which deexcite the energy levels E_i in ^{131}Cs. The E_γ uncertainty in strong γ-ray energies is less than 0.3 keV; for weak γ-ray energies, about 0.5 keV. The DCO values in column 6 are obtained from gates on stretched $E2$ transitions.

E_γ (keV)	E_i (keV)	Relative intensity	Band	$I_i^\pi \rightarrow I_f^\pi$	DCO	Polarization
78.2	78	405(21)	B5→B6	$7/2^+ \rightarrow 5/2^+$		
81.1	2816	8.3(12)	B10→B6	$23/2^- \rightarrow 21/2^+$		
95.4	2876	9.0(14)	B8→B8	$23/2^+ \rightarrow 21/2^+$		
98.7	3820	1.88(39)	B10→B11	$27/2^- \rightarrow 25/2^-$		
109.7	4736	0.43(10)	B8→B8	$33/2^+ \rightarrow 31/2^+$		
120.5	2344	4.06(56)	B12→B12	$19/2^- \rightarrow 17/2^-$		
131.3	2687	7.0(8)	B2→B2	$19/2^+ \rightarrow 17/2^+$	0.41(8)	
133.0	3858	0.40(6)	B8→B10	$29/2^+ \rightarrow 27/2^-$		
140.3	2876	90(5)	B8→B6	$23/2^+ \rightarrow 21/2^+$	0.66(7)	−0.05(1)
148.3	2836	7.0(8)	B2→B2	$21/2^+ \rightarrow 19/2^+$	0.30(7)	
154.8	3820	10.9(10)	B11→B11	$27/2^- \rightarrow 25/2^-$	0.45(9)	
155.3	2816	10(1)	B10→B10	$23/2^- \rightarrow 21/2^-$	0.45(11)	
159.0	776	3.27(39)	B10→B6	$11/2^- \rightarrow 9/2^+$		
162.0	1310	1.18(18)	B10→B6	$15/2^- \rightarrow 13/2^+$		
166.6	3043	58.3(40)	B7→B8	$25/2^+ \rightarrow 23/2^+$	0.79(12)	
167.0	4146	7.6(9)	B2→B3	$29/2^+ \rightarrow 27/2^+$		−0.07(3)
188.9	3858	9.8(13)	B8→B8	$29/2^+ \rightarrow 27/2^+$		
192.7	2875	2.56(38)	B1→B1	$19/2^+ \rightarrow 17/2^+$	0.42(11)	
193.2	3724	3.4(5)	B2→B3	$27/2^+ \rightarrow 25/2^+$	0.35(9)	
203.7	3725	15(2)	B10→B10	$27/2^- \rightarrow 25/2^-$	0.48(9)	
206.0	$550 + x$		B4→B4	$13/2^+ \rightarrow 11/2^+$		
223.1	3059	45(3)	B2→B2	$23/2^+ \rightarrow 21/2^+$	0.50(8)	
226.4	2155	4.6(6)	B5→B6	$19/2^+ \rightarrow 17/2^+$		
231.8	1637	16.6(17)	B12→B10	$15/2^- \rightarrow 13/2^-$		
261.0	2544	28.7(23)	B13→B13	$19/2^- \rightarrow 17/2^-$	0.64(10)	
261.3	3725	19.4(21)	B10→B11	$27/2^- \rightarrow 25/2^-$	0.64(12)	
266.0	$344 + x$		B4→B4	$11/2^+ \rightarrow 9/2^+$		
273.8	2223	26(3)	B12→B12	$17/2^- \rightarrow 15/2^-$	0.45(8)	
278.3	3059	31(2)	B2→B8	$23/2^+ \rightarrow 21/2^+$		
278.8	776	740(29)	B10→B6	$11/2^- \rightarrow 9/2^+$	0.52(4)	
279.6	2035		B1→B1	$15/2^+ \rightarrow 13/2^+$		
285.6	4011	35(3)	B11→B10	$29/2^- \rightarrow 27/2^-$	0.45(6)	
288.2	3164	62.4(37)	B8→B8	$25/2^+ \rightarrow 23/2^+$	0.52(6)	−0.04(2)
293.0	3160	6.2(8)	B14→B14	$23/2^- \rightarrow 21/2^-$	0.60(13)	
298.7	3033	4.8(6)	B5→B6	$23/2^+ \rightarrow 21/2^+$		
303.0	3907	13.4(13)	B14→B14	$27/2^- \rightarrow 25/2^-$		
303.0	2526	16.7(17)	B14→B14	$19/2^- \rightarrow 17/2^-$	0.41(8)	
305.0	5530	5.0(8)	B3→B3	$35/2^+ \rightarrow 33/2^+$	0.57(13)	
308.3	3724	30(2)	B2→B2	$27/2^+ \rightarrow 25/2^+$	0.53(13)	
315.8	4655	1.71(34)	B2→B3	$31/2^+ \rightarrow 29/2^+$		
318.8	4044	1.95(35)	B9→B10	$27/2^- \rightarrow 27/2^-$	0.60(15)	
321.0	2544	37.2(26)	B13→B12	$19/2^- \rightarrow 17/2^-$	0.72(12)	
321.5	2345	6.0(9)	B12→B10	$19/2^- \rightarrow 17/2^-$		
331.7	2677	53(4)	B12→B12	$21/2^- \rightarrow 19/2^-$	0.56(6)	
334.7	2284	33.3(33)	B13→B12	$17/2^- \rightarrow 15/2^-$	0.62(6)	
341.0	5246	11(2)	B11→B11	$35/2^- \rightarrow 33/2^-$	0.72(18)	
341.0	2867	6.7(8)	B14→B14	$21/2^- \rightarrow 19/2^-$		
341.6	3972	9.0(13)	B5→B6	$27/2^+ \rightarrow 25/2^+$	0.46(10)	
345.5	6202	2.08(21)	B11→B11	$(39/2^-) \rightarrow 37/2^-$	0.54(12)	
347.0	2891	39.7(28)	B13→B13	$21/2^- \rightarrow 19/2^-$	0.70(14)	
347.5	3164	0.31(6)	B8→B10	$25/2^+ \rightarrow 23/2^-$		
348.0	4913	16.4(16)	B11→B11	$33/2^- \rightarrow 31/2^-$	0.60(12)	
349.0	3240	8.2(12)	B13→B13	$23/2^- \rightarrow 21/2^-$	0.67(14)	
352.2	3873	0.55(14)	B12→B10	$27/2^- \rightarrow 25/2^-$		
356.1	3416	49(3)	B2→B2	$25/2^+ \rightarrow 23/2^+$	0.65(10)	

TABLE I. *(Continued.)*

E_γ (keV)	E_i (keV)	Relative intensity	Band	$I_i^\pi \rightarrow I_f^\pi$	DCO	Polarization
359.5	5264	22.2(21)	B11→B11	$(35/2^-) \rightarrow 33/2^-$	0.52(5)	
360.0	4339	3.86(39)	B3→B3	$29/2^+ \rightarrow 27/2^+$	0.62(9)	
360.7	3426	15.6(17)	B12→B12	$25/2^- \rightarrow 23/2^-$		
366.0	4705	1.29(19)	B3→B3	$31/2^+ \rightarrow 29/2^+$	0.59(13)	
370.7	2345	8.6(10)	B12→B10	$19/2^- \rightarrow 19/2^-$		
372.0	1148	3.3(4)	B6→B10	$13/2^+ \rightarrow 11/2^-$		
375.4	4386	48.2(52)	B11→B11	$31/2^- \rightarrow 29/2^-$	0.47(8)	−0.1(2)
381.3	3416	7.3(9)	B2→B5	$25/2^+ \rightarrow 23/2^+$		
388.1	3065	10.2(12)	B12→B12	$23/2^- \rightarrow 21/2^-$	0.58(9)	
390.4	4011	66.2(65)	B11→B11	$29/2^- \rightarrow 27/2^-$	0.58(9)	−0.06(4)
394.8	2344	68(4)	B12→B12	$19/2^- \rightarrow 15/2^-$	1.18(14)	
400.1	3465	5.9(11)	B11→B12	$25/2^- \rightarrow 23/2^-$		
404.5	3065	4.5(6)	B12→B10	$23/2^- \rightarrow 21/2^-$		
405.0	$749 + x$		B4→B4	$13/2^+ \rightarrow 11/2^+$		
414.6	2345	13.9(14)	B12→B6	$19/2^- \rightarrow 17/2^+$	0.64(12)	
417.3	496	65(4)	B6→B5	$9/2^+ \rightarrow 7/2^+$		
419.4	4293	5.17(52)	B12→B12	$29/2^- \rightarrow 27/2^-$		
421.6	4146	27.8(19)	B2→B2	$29/2^+ \rightarrow 27/2^+$	0.63(10)	
424.7	5080	8.1(10)	B2→B2	$33/2^+ \rightarrow 31/2^+$	0.57(10)	
426.2	4719	7.4(9)	B12→B12	$31/2^- \rightarrow 29/2^-$	0.57(10)	
427.0	3667	5.9(8)	B13→B13	$25/2^- \rightarrow 23/2^-$	0.54(10)	
429.0	5959	4.13(61)	B3→B3	$37/2^+ \rightarrow 35/2^+$	0.46(9)	
443.2	3762		B1→B1	$23/2^+ \rightarrow 21/2^+$		
444.0	3604	7.1(10)	B14→B14	$25/2^- \rightarrow 23/2^-$	0.54(17)	
446.1	3873	7.34(76)	B12→B12	$27/2^- \rightarrow 25/2^-$		
449.1	3979	8.2(9)	B3→B3	$27/2^+ \rightarrow 25/2^+$		
449.1	5530	4.93(69)	B3→B2	$35/2^+ \rightarrow 33/2^+$		
457.0	$801 + x$		B4→B4	$15/2^+ \rightarrow 11/2^+$		
464.0	3280	5.22(63)	B9→B10	$23/2^- \rightarrow 23/2^-$	0.86(15)	
471.0	3530	16.6(13)	B3→B2	$25/2^+ \rightarrow 23/2^+$		
472.0	$550 + x$		B4→B4	$13/2^+ \rightarrow 9/2^+$		
472.0	3565	10.6(11)	B5→B5	$27/2^+ \rightarrow 23/2^+$	0.87(14)	
479.2	4348	14.7(15)	B7→B7	$31/2^+ \rightarrow 29/2^+$	0.64(12)	
484.3	3319	1.61(29)	B1→B1	$21/2^+ \rightarrow 19/2^+$	0.46(12)	
485.8	4872	29.8(30)	B11→B11	$33/2^- \rightarrow 31/2^-$	0.62(10)	
490.0	4348	6.46(78)	B8→B8	$31/2^+ \rightarrow 29/2^+$	0.65(13)	
495.9	496	1000(40)	B6→B6	$9/2^+ \rightarrow 5/2^+$		
503.7	3669	5.6(8)	B14→B10	$19/2^- \rightarrow 17/2^-$	0.52(10)	
504.8	3669	5.73(74)	B8→B8	$27/2^+ \rightarrow 25/2^+$	0.46(8)	
509.3	4655	5.4(7)	B2→B2	$31/2^+ \rightarrow 29/2^+$	0.60(10)	
514.0	$1263 + x$		B4→B4	$17/2^+ \rightarrow 13/2^+$		
516.0	5388	17.2(17)	B11→B11	$35/2^- \rightarrow 33/2^-$	0.43(7)	
518.4	4905	25.8(29)	B11→B11	$33/2^- \rightarrow 31/2^-$	0.54(6)	
519.0	5225	3.92(51)	B3→B3	$33/2^+ \rightarrow 31/2^+$	0.62(12)	
521.7	2544	6.7(8)	B13→B10	$19/2^- \rightarrow 17/2^-$		
523.0	1833	15(2)		$15/2^- \rightarrow 15/2^-$	0.62(11)	
523.0	2356	22(2)		$(19/2^-) \rightarrow 15/2^-$		
531.3	1148	25(2)	B6→B5	$13/2^+ \rightarrow 11/2^+$	0.64(10)	
532.3	2687	18(2)	B2→B5	$19/2^+ \rightarrow 17/2^+$	0.64(12)	
533.2	1310	590(30)	B10→B10	$15/2^- \rightarrow 11/2^-$	0.99(10)	
537.6	617	388(19)	B5→B5	$11/2^+ \rightarrow 7/2^+$		
543.3	1949	106(7)	B12→B10	$15/2^- \rightarrow 13/2^-$	0.45(5)	
544.0	4451	5.4(9)	B14→B14	$(29/2^-) \rightarrow 27/2^-$		
546.5	2891	19.3(19)	B13→B12	$21/2^- \rightarrow 19/2^-$	0.96(15)	
546.8	4011	25.6(23)	B11→B11	$29/2^- \rightarrow 25/2^-$		
550.4	3593	35.2(28)	B7→B7	$27/2^+ \rightarrow 25/2^+$	0.62(9)	
552.7	2526	53.7(32)	B14→B10	$19/2^- \rightarrow 19/2^-$	0.58(6)	

TABLE I. *(Continued.)*

E_γ (keV)	E_i (keV)	Relative intensity	Band	$I_i^\pi \rightarrow I_f^\pi$	DCO	Polarization
553.0	5005	2.73(49)	B14→B14	$(31/2^-) \rightarrow (29/2^-)$		
554.2	4565	28.9(35)	B11→B11	$31/2^- \rightarrow 29/2^-$	0.38(7)	
559.0	4705	3.4(7)	B3→B2	$31/2^+ \rightarrow 29/2^+$	0.53(13)	
561.0	3725	6.05(60)	B10→B8	$27/2^- \rightarrow 25/2^+$		
562.6	3979	7.1(8)	B3→B2	$27/2^+ \rightarrow 25/2^+$	0.48(8)	
563.2	3240	12.2(16)	B13→B12	$23/2^- \rightarrow 21/2^-$		
566.0	2573	9.0(10)	B9→B9	$19/2^- \rightarrow 15/2^-$	0.87(14)	
569.7	5225	1.5(4)	B3→B2	$33/2^+ \rightarrow 31/2^+$	0.63(22)	
576.8	2526	10.6(11)	B14→B12	$19/2^- \rightarrow 15/2^-$		
578.9	2735	25(1)	B6→B5	$21/2^+ \rightarrow 19/2^+$	0.47(7)	
592.5	5857	4.24(50)	B11→B11	$37/2^- \rightarrow 35/2^-$	0.53(9)	
594.8	2544	33.7(24)	B13→B12	$19/2^- \rightarrow 15/2^-$	0.86(10)	
597.3	3631	15.7(24)	B6→B5	$25/2^+ \rightarrow 23/2^+$		
599.7	2573	19.1(19)	B9→B10	$19/2^- \rightarrow 19/2^-$		
602.1	3667	6.2(4)	B13→B12	$25/2^- \rightarrow 23/2^-$	0.51(7)	
604.1	1929	66(4)	B6→B5	$17/2^+ \rightarrow 15/2^+$	0.41(5)	
607.4	2642	4.8(7)	B1→B1	$17/2^+ \rightarrow 15/2^+$	0.56(12)	
608.0	2891	28.2(22)	B13→B13	$21/2^- \rightarrow 17/2^-$	0.78(15)	
614.6	4339	2.0(4)	B3→B2	$29/2^+ \rightarrow 27/2^+$	0.58(15)	
616.8	2022	20(2)	B10→B10	$17/2^- \rightarrow 13/2^-$	0.95(17)	
619.1	1929	11(2)	B6→B10	$17/2^+ \rightarrow 15/2^-$		
626.1	2555	0.48(12)	B2→B3	$17/2^+ \rightarrow 17/2^+$		
626.4	3669	12.8(12)	B8→B8	$27/2^+ \rightarrow 25/2^+$	0.46(9)	
629.0	1405	160(16)	B10→B10	$13/2^- \rightarrow 11/2^-$	0.38(5)	
634.0	3160	20.2(28)	B14→B14	$23/2^- \rightarrow 19/2^-$		
637.6	2660	8.0(10)	B10→B10	$21/2^- \rightarrow 17/2^-$	0.90(15)	
639.0	1949	40.2(28)	B12→B10	$15/2^- \rightarrow 15/2^-$		
644.0	2867	20.3(16)	B14→B14	$21/2^- \rightarrow 17/2^-$	0.72(10)	
646.0	$1395 + x$		B4→B4	$19/2^+ \rightarrow 15/2^+$		
648.1	3465	36.7(26)	B11→B10	$25/2^- \rightarrow 23/2^-$	0.56(14)	
650.8	1148	370(19)	B6→B6	$13/2^+ \rightarrow 9/2^+$	1.02(14)	
653.8	2677	3.8(6)	B12→B10	$21/2^- \rightarrow 17/2^-$		
663.0	1973	370(19)	B10→B10	$19/2^- \rightarrow 15/2^-$	1.12(12)	
664.5	3724	8.9(9)	B2→B2	$27/2^+ \rightarrow 23/2^+$		
668.0	2891	10(1)	B13→B12	$21/2^- \rightarrow 17/2^-$		
677.0	3319		B1→B1	$21/2^+ \rightarrow 17/2^+$		
680.0	$1481 + x$		B4→B4	$19/2^+ \rightarrow 15/2^+$		
680.6	2836	1.0(2)	B2→B5	$21/2^+ \rightarrow 19/2^+$		
686.3	2660	48(5)	B10→B10	$21/2^- \rightarrow 19/2^-$	0.43(6)	
693.2	3858	30.3(24)	B8→B8	$29/2^+ \rightarrow 25/2^+$		
694.6	3530	3.41(41)	B3→B2	$25/2^+ \rightarrow 21/2^+$		
696.0	$1246 + x$		B4→B4	$17/2^+ \rightarrow 13/2^+$		
697.3	2007	15.6(15)	B9→B10	$15/2^- \rightarrow 15/2^-$	0.34(4)	
702.8	2677	11(1)	B12→B10	$21/2^- \rightarrow 19/2^-$	0.45(7)	
704.3	3521	7.0(8)	B10→B10	$25/2^- \rightarrow 23/2^-$		
704.6	3869	16.2(15)	B7→B8	$29/2^+ \rightarrow 25/2^+$		
706.3	3280	3.92(47)	B9→B9	$23/2^- \rightarrow 19/2^-$	1.06(17)	
707.6	1325	371(19)	B5→B5	$15/2^+ \rightarrow 11/2^+$	1.13(15)	
707.7	2345	7.9(7)	B12→B12	$19/2^- \rightarrow 15/2^-$	0.82(12)	0.07(2)
712.4	2022	63(4)	B10→B10	$17/2^- \rightarrow 15/2^-$	0.44(7)	
719.8	3065	23(2)	B12→B12	$23/2^- \rightarrow 19/2^-$	0.70(8)	
720.1	2876	37.2(26)	B8→B5	$23/2^+ \rightarrow 19/2^+$	0.85(13)	
726.0	4705	1.15(17)	B3→B3	$31/2^+ \rightarrow 27/2^+$		
728.0	3429	14.6(18)	B15→B15	$23/2^- \rightarrow 19/2^-$	0.86(12)	
730.2	4146	4.82(58)	B2→B2	$29/2^+ \rightarrow 25/2^+$	0.81(11)	
734.0	5959	0.86(22)	B3→B3	$37/2^+ \rightarrow 33/2^+$	0.81(24)	
737.0	3604	10.4(10)	B14→B14	$25/2^- \rightarrow 21/2^-$	0.92(13)	

TABLE I. *(Continued.)*

E_γ (keV)	E_i (keV)	Relative intensity	Band	$I_i^\pi \rightarrow I_f^\pi$	DCO	Polarization
747.0	3907	23.9(19)	B14→B14	$27/2^- \rightarrow 23/2^-$	0.72(13)	
748.7	3426	15.5(16)	B12→B12	$25/2^- \rightarrow 21/2^-$	0.94(14)	
750.0	4179		B15→B15	$(27/2^-) \rightarrow 23/2^-$		
755.0	4348	6.8(10)	B7→B7	$31/2^+ \rightarrow 27/2^+$	0.77(17)	
761.3	2735	7(1)	B6→B10	$21/2^+ \rightarrow 19/2^-$		
764.0	4044	3.42(48)	B9→B9	$27/2^- \rightarrow 23/2^-$	0.84(15)	
765.6	3426	6.4(10)	B12→B10	$25/2^- \rightarrow 21/2^-$		
765.8	4386	22(2)	B11→B11	$31/2^- \rightarrow 27/2^-$	0.89(16)	
769.0	4386		B8→B8	$31/2^+ \rightarrow 29/2^+$		
774.0	$2020 + x$		B4→B4	$21/2^+ \rightarrow 17/2^+$		
776.0	3667	7.8(11)	B13→B13	$25/2^- \rightarrow 21/2^-$	0.92(17)	
780.4	1929	320(13)	B6→B6	$17/2^+ \rightarrow 13/2^+$	1.01(10)	
785.0	4642	2.4(6)	B10→B8	$31/2^- \rightarrow 29/2^+$		
793.0	3669	26.8(22)	B8→B8	$27/2^+ \rightarrow 23/2^+$	1.0(2)	
800.1	2835		B1→B1	$19/2^+ \rightarrow 15/2^+$		
803.7	3820	146(7)	B11→B10	$27/2^- \rightarrow 23/2^-$		0.03(2)
804.1	3465	31.2(25)	B11→B10	$25/2^- \rightarrow 21/2^-$		
805.8	2735	307(15)	B6→B6	$21/2^+ \rightarrow 17/2^+$	0.99(10)	
807.3	3873	14.5(16)	B12→B12	$27/2^- \rightarrow 23/2^-$		
808.6	4339	1.85(22)	B3→B3	$29/2^+ \rightarrow 25/2^+$	1.0(2)	
815.2	3858	19.9(20)	B8→B7	$29/2^+ \rightarrow 25/2^+$		
825.0	$2306 + x$		B4→B4	$23/2^+ \rightarrow 19/2^+$		
825.0	5530	4.29(51)	B3→B3	$35/2^+ \rightarrow 31/2^+$	0.83(13)	
825.9	3869	39.4(28)	B7→B7	$29/2^+ \rightarrow 25/2^+$	1.17(18)	
830.0	2155	201(10)	B5→B5	$19/2^+ \rightarrow 15/2^+$	0.95(9)	
842.8	2816	242(12)	B10→B10	$23/2^- \rightarrow 19/2^-$	1.07(16)	
843.5	2555	31(2)	B2→B2	$17/2^+ \rightarrow 13/2^+$		
846.2	4719	13.8(14)	B12→B12	$31/2^- \rightarrow 27/2^-$	0.90(19)	
847.0	4451	7.8(11)	B14→B14	$(29/2^-) \rightarrow 25/2^-$		
851.3	2781	82(5)	B8→B6	$21/2^+ \rightarrow 17/2^+$	1.25(17)	
854.0	$2874 + x$		B4→B4	$25/2^+ \rightarrow 21/2^+$		
860.8	3521	7.0(10)	B10→B10	$25/2^- \rightarrow 21/2^-$	0.98(18)	
866.2	4293	10(1)	B12→B12	$29/2^- \rightarrow 25/2^-$	0.86(16)	
866.9	4736	8.5(10)	B8→B8	$33/2^+ \rightarrow 29/2^+$		
874.7	5530	2.7(4)	B3→B2	$35/2^+ \rightarrow 31/2^+$	0.74(21)	
877.3	4736	26(2)	B8→B8	$33/2^+ \rightarrow 29/2^+$	0.92(15)	
877.4	5264	21(2)	B11→B11	$(35/2^-) \rightarrow 31/2^-$		
877.5	3033	65(4)	B5→B5	$23/2^+ \rightarrow 19/2^+$	0.97(11)	
879.0	5959	1.17(23)	B3→B2	$37/2^+ \rightarrow 33/2^+$		
879.0	5738	4.8(7)	B8→B7	$37/2^+ \rightarrow 33/2^+$		
886.0	5225	1.18(20)	B3→B3	$33/2^+ \rightarrow 29/2^+$	0.88(21)	
887.0	2642	4.9(8)	B1→B1	$17/2^+ \rightarrow 13/2^+$	0.86(15)	
893.8	4905	6.4(6)	B11→B11	$33/2^- \rightarrow 29/2^-$		
895.5	3240	8.4(12)	B13→B12	$23/2^- \rightarrow 19/2^-$	0.83(16)	
896.0	3631	15(2)	B6→B6	$25/2^+ \rightarrow 21/2^+$	0.87(14)	
898.3	2223	13(1)	B14→B5	$17/2^- \rightarrow 15/2^+$	0.77(15)	
902.6	3059	17.6(14)	B2→B5	$23/2^+ \rightarrow 19/2^+$	1.08(22)	0.14(6)
906.0	5254	11.1(11)	B7→B7	$(35/2^+) \rightarrow 31/2^+$		
906.2	2836	18(1)	B2→B6	$21/2^+ \rightarrow 17/2^+$	0.96(11)	0.11(6)
908.5	3725	58.6(29)	B10→B10	$27/2^- \rightarrow 23/2^-$	1.39(17)	
917.0	4642	9.0(9)	B10→B10	$31/2^- \rightarrow 27/2^-$	1.12(20)	
930.9	4655	6.2(8)	B2→B2	$31/2^+ \rightarrow 27/2^+$	0.83(14)	
934.0	5080	10.4(15)	B2→B2	$33/2^+ \rightarrow 29/2^+$	0.83(15)	
938.0	3093	22.2(18)	B5→B5	$23/2^+ \rightarrow 19/2^+$	1.02(17)	
938.0	6202	8.3(8)	B11→B11	$(39/2^-) \rightarrow (35/2^-)$		
938.3	3972	6.4(9)	B5→B5	$27/2^+ \rightarrow 23/2^+$	0.86(12)	
952.0	5857	5.6(5)	B11→B11	$37/2^- \rightarrow 33/2^-$	0.93(18)	

TABLE I. *(Continued.)*

E_γ (keV)	E_i (keV)	Relative intensity	Band	$I_i^\pi \rightarrow I_f^\pi$	DCO	Polarization
957.0	4626	7.4(9)	B8→B8	$31/2^+ \rightarrow 27/2^+$	0.76(14)	
958.0	4384	7.4(9)	B12→B12	$29/2^- \rightarrow 25/2^-$	0.87(14)	
972.0	4830	7.8(9)	B8→B8	$33/2^+ \rightarrow 29/2^+$	0.87(9)	
983.0	4856	5.3(8)	B12→B12	$31/2^- \rightarrow 27/2^-$	0.97(10)	
988.1	4858	19.5(19)	B7→B7	$33/2^+ \rightarrow 29/2^+$	0.98(8)	
990.2	3667	6.0(9)	B13→B12	$25/2^- \rightarrow 21/2^-$	0.89(18)	
993.7	4719	4.7(7)	B12→B10	$31/2^- \rightarrow 27/2^-$		
999.4	4858	5.7(7)	B7→B8	$33/2^+ \rightarrow 29/2^+$		
1001.2	5738	15(2)	B8→B8	$37/2^+ \rightarrow 33/2^+$		
1014.0	6752	19.1(19)	B8→B8	$41/2^+ \rightarrow 37/2^+$	0.99(15)	
1039.0	7791	11.1(16)	B8→B8	$45/2^+ \rightarrow 41/2^+$	1.03(14)	
1048.0	5341	7.7(12)	B12→B12	$33/2^- \rightarrow 29/2^-$	0.88(12)	
1057.1	1833	10.5(10)		$15/2^- \rightarrow 11/2^-$	0.88(16)	
1057.2	3873	8.0(11)	B12→B10	$27/2^- \rightarrow 23/2^-$	0.88(15)	
1091.6	3065	9.4(11)	B12→B10	$23/2^- \rightarrow 19/2^-$	0.89(13)	
1093.4	1711	19(2)	B2→B2	$13/2^+ \rightarrow 11/2^+$	0.63(12)	
1098.0	5005	7.4(11)	B14→B14	$(31/2^-) \rightarrow 27/2^-$		
1138.4	1755	9.2(11)	B1→B5	$13/2^+ \rightarrow 11/2^+$	0.50(11)	
1148.0	8939	1.58(25)	B8→B8	$(49/2^+) \rightarrow 45/2^+$		
1163.8	3319	4.4(6)	B1→B1	$21/2^+ \rightarrow 19/2^+$	0.61(15)	
1173.3	1949	8.4(10)	B12→B10	$15/2^- \rightarrow 11/2^-$	0.84(13)	
1184.0	6042	1.0(2)	B7→B7	$37/2^+ \rightarrow 33/2^+$	0.82(19)	
1216.3	2526	9.2(11)	B14→B10	$19/2^- \rightarrow 15/2^-$	0.85(15)	
1228.0	4044	8.2(8)	B9→B10	$27/2^- \rightarrow 23/2^-$	0.73(12)	
1228.5	2555	17(1)	B2→B5	$17/2^+ \rightarrow 15/2^+$	0.55(6)	−0.06(4)
1231.1	2007	4.7(6)	B9→B10	$15/2^- \rightarrow 11/2^-$	0.78(16)	
1234.3	2544	5.4(6)	B13→B10	$19/2^- \rightarrow 15/2^-$	1.25(25)	
1263.3	2573	7.8(9)	B9→B10	$19/2^- \rightarrow 15/2^-$	0.83(17)	
1306.4	3280	5.07(51)	B9→B10	$23/2^- \rightarrow 19/2^-$	0.76(11)	
1317.3	2642	11.6(14)	B1→B5	$17/2^+ \rightarrow 15/2^+$	0.50(9)	
1359.0	2507	4.01(56)	B6→B6	$(17/2^+) \rightarrow 13/2^+$		
1363.3	4179	2.74(41)	B15→B10	$(27/2^-) \rightarrow 23/2^-$		
1367.0	2692	3.51(53)	B5→B5	$(19/2^+) \rightarrow 15/2^+$		
1391.3	2701	4.48(54)	B15→B10	$19/2^- \rightarrow 15/2^-$	0.78(14)	
1418.0	2035	4.9(7)	B1→B5	$15/2^+ \rightarrow 11/2^+$	0.76(13)	
1455.7	3429	3.4(5)	B15→B10	$23/2^- \rightarrow 19/2^-$	0.78(11)	
1510.0	2835	3.29(39)	B1→B5	$19/2^+ \rightarrow 15/2^+$	0.86(15)	
1607.0	3762	2.97(53)	B1→B5	$23/2^+ \rightarrow 19/2^+$	0.81(20)	

A. Positive-parity bands

1. B1, B5, and B6 bands

The previous observation of the B5 and B6 bands comprising $\Delta I = 2$ cascades with transitions 537.6–707.6–830.0–877.5–938.3 keV and 495.6–650.8–780.4–805.8 keV, respectively, has been confirmed in the present work. They have been interpreted as built on the $\pi g_{7/2}$ and $\pi d_{5/2}$ orbitals, respectively [24]. A new $E2$ transition with energy 896.0 keV has been identified in coincidence with the second cascade. This has been placed at the top of B6, thereby extending it to an excitation energy of 3631 keV and $I^\pi = 25/2^+$. In addition, new transitions have been identified; e.g., the 1359.0 and 1367.0 keV $E2$ transitions side-feed the $13/2^+$ level of band B6 and $15/2^+$ level of band B5, respectively. Another cascade with transitions 938.0–472.0 keV is found to feed at the $I^\pi = 19/2^+$ level of band B5 (see Fig. 3). A detailed analysis of different gated spectra in coincidence with transitions in B5, lead us to place the $\Delta I = 2$ transitions with energies 1418.0, 1510.0, and 1607.0 keV, and the strong $\Delta I = 1$ transitions with energies 1138.4, 1317.3, and 1163.8 keV directly feeding the different levels of band B5, thus establishing the new B1 band up to $I^\pi = 23/2^+$. The intraband $\Delta I = 1$ transitions of energies 192.7 keV ($19/2^+ \rightarrow 17/2^+$) and 279.6 keV ($15/2^+ \rightarrow 13/2^+$) are also observed. The gated spectrum showing the connecting transitions between B1 and B5 bands is given in Fig. 3. Spin assignments to the levels of band B1 have been done on the basis of the DCO ratios of the transitions linking the levels of the positive-parity band $\pi g_{7/2}$ (B5). The in-band transitions are very weak compared to the out-of-band transitions to the highest observed spins. The decay pattern of this band is

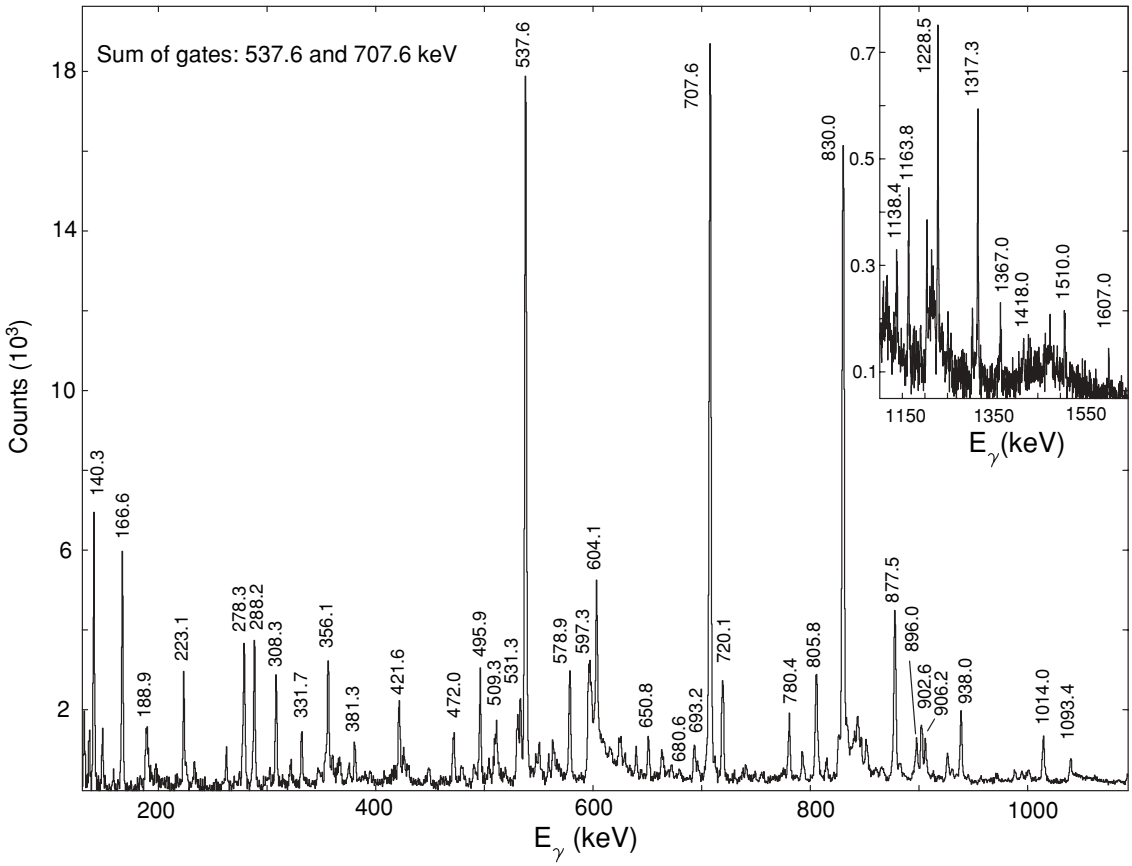

FIG. 3. γ-ray summed coincidence spectrum with gates on the 537.6 and 707.6 keV transitions of band B5.

similar to the γ-vibrational band in nearby even-even nuclei. Therefore the bandhead could be tentatively assigned to have positive parity.

2. B2 and B3 bands

The positive-parity band B2 comprises mainly strong $\Delta I = 1$ dipole transitions and decays into levels of the $\pi g_{7/2}$ (B5) and $\pi d_{5/2}$ (B6) bands. The 424.7 keV, $\Delta I = 1$ and 934.0 keV, $\Delta I = 2$ transitions are added at the top. The spin-parity of the new level has been inferred from the DCO ratio of the crossover 934.0 keV and also the 424.7 transitions (see Table I). The new 680.6 keV ($21/2^+ \rightarrow 19/2^+$, $M1$) transition and the cascade of 843.5 keV ($17/2^+ \rightarrow 13/2^+$, $E2$) and 1093.4 keV ($13/2^+ \rightarrow 11/2^+$, $M1$) transitions are added to the earlier observed decay pattern from lower levels of band B2 to band B5. A new weakly populated positive-parity band B3 is established up to $I^\pi = 37/2^+$ in this work. The coincidence gated spectrum for this band is shown in Fig. 4(a). Its bandhead lying at 3530 keV has been assigned $I^\pi = 25/2^+$. The 315.8, 167.0, 193.2, and 381.3 keV dipole transitions are decaying from higher levels of band B2 to corresponding levels of band B3. The dipole transitions 449.1, 569.7, 559.0, 614.6, 562.6, and 471.0 keV from levels in B3 band have been found to feed the B2 band. In addition, the $\Delta I = 2$ transitions 874.7, 879.0, and 694.6 keV from band B3 are also feeding levels in the B2 band. These features suggest the same positive parity for both bands B2 and B3.

3. B7 and B8 bands

The previously known band B8 has been extended with the addition of three new levels up to $I^\pi = (49/2^+)$. Similarly, the previously known band B7 has been extended through the addition of an $E2$ transition of energy 1184.0 keV at the top and extends to the 6042 keV ($I^\pi = 37/2^+$) level. The likely unfavored signature partners of bands B7 and B8 have been observed for the first time. The linking dipole transitions from these bands to the favored counterparts have also been observed. A new 879 keV $E2$ transition has been observed from the $I^\pi = 37/2^+$ level in B8 band to the $I^\pi = 33/2^+$ level in B7. Additional transitions 972.0 and 490.0 keV feed the 3858 keV ($I^\pi = 29/2^+$) level in the B8 band. The gated spectrum for these bands is shown in Fig. 4(b). In the present work, the $\Delta I = 1$ character of the already observed transitions 166.6 and 140.3 keV has been confirmed through the DCO ratio, and the present polarization measurements have established the $M1$ character of the 140.3 keV transition.

4. B4 band

Band B4 consisting of two $\Delta I = 2\,\gamma$ sequences, namely, 472.0–696.0–774.0–854.0 keV and 457.0–680.0–825.0 keV, has been observed in coincidence with only the 78.2 keV transition. In addition, two connecting transitions with energies 266.0 and 206.0 keV with $\Delta I = 1$ have also been identified between the above sequences. The gated spectrum for this band

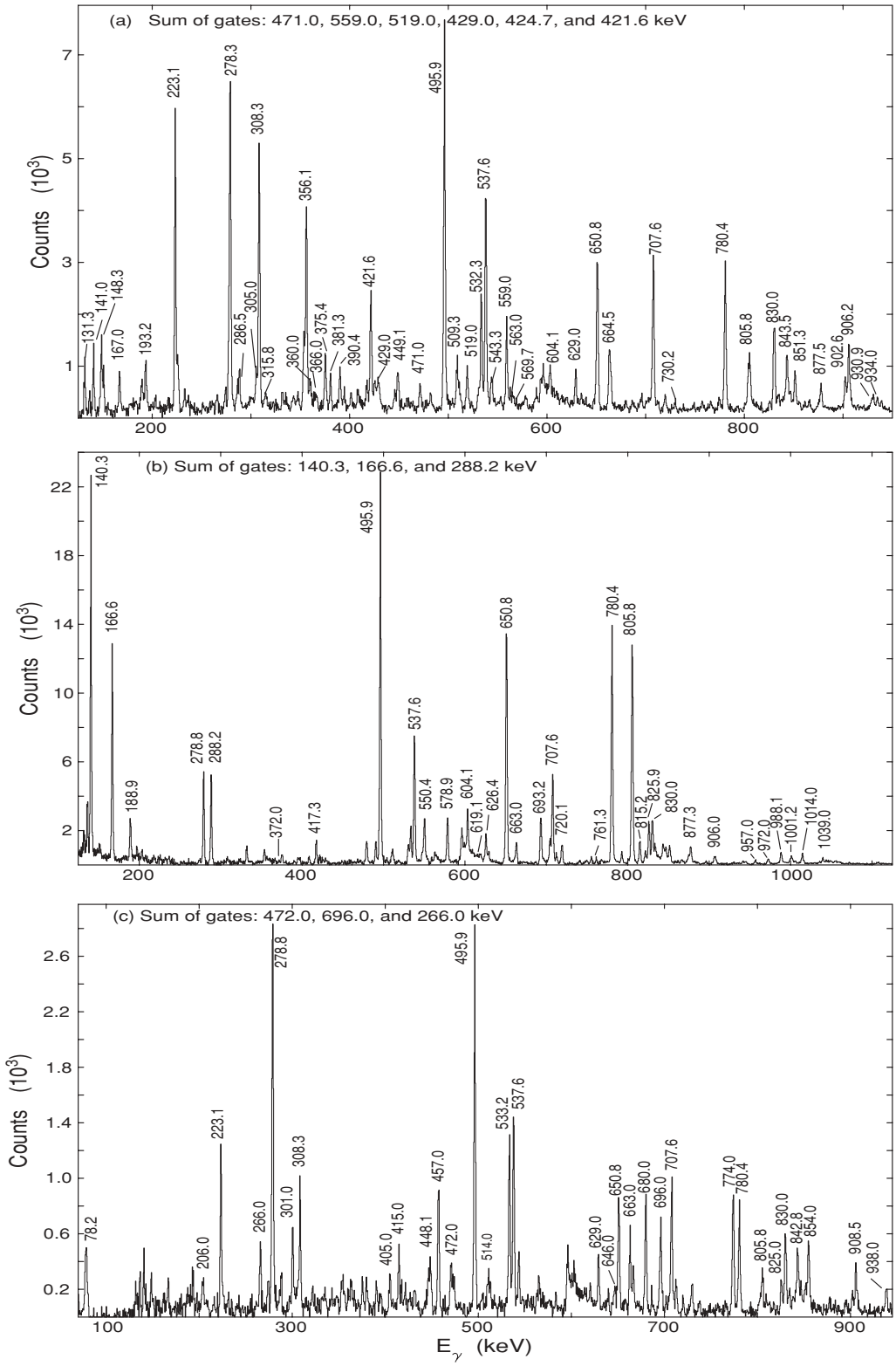

FIG. 4. γ-ray summed coincidence spectra with gates on the mentioned transitions depicting γ transitions related mainly to positive-parity bands (a) B2 and B3, (b) B7 and B8, and (c) B4.

is shown in Fig. 4(c). Besides the 78.2 keV transition, no other linking transition has been established between B4 and any other bands of ^{131}Cs. Therefore, band B4 is tentatively assigned to ^{131}Cs. However, a similar band structure based on the $\pi g_{9/2}$ configuration has been observed in $^{119-127}$Cs isotopes [29]. The excitation energy systematics of these lighter odd Cs isotopes suggest that the bandhead of B4 has an excitation energy around 1.3 MeV and a high-K configuration. This may

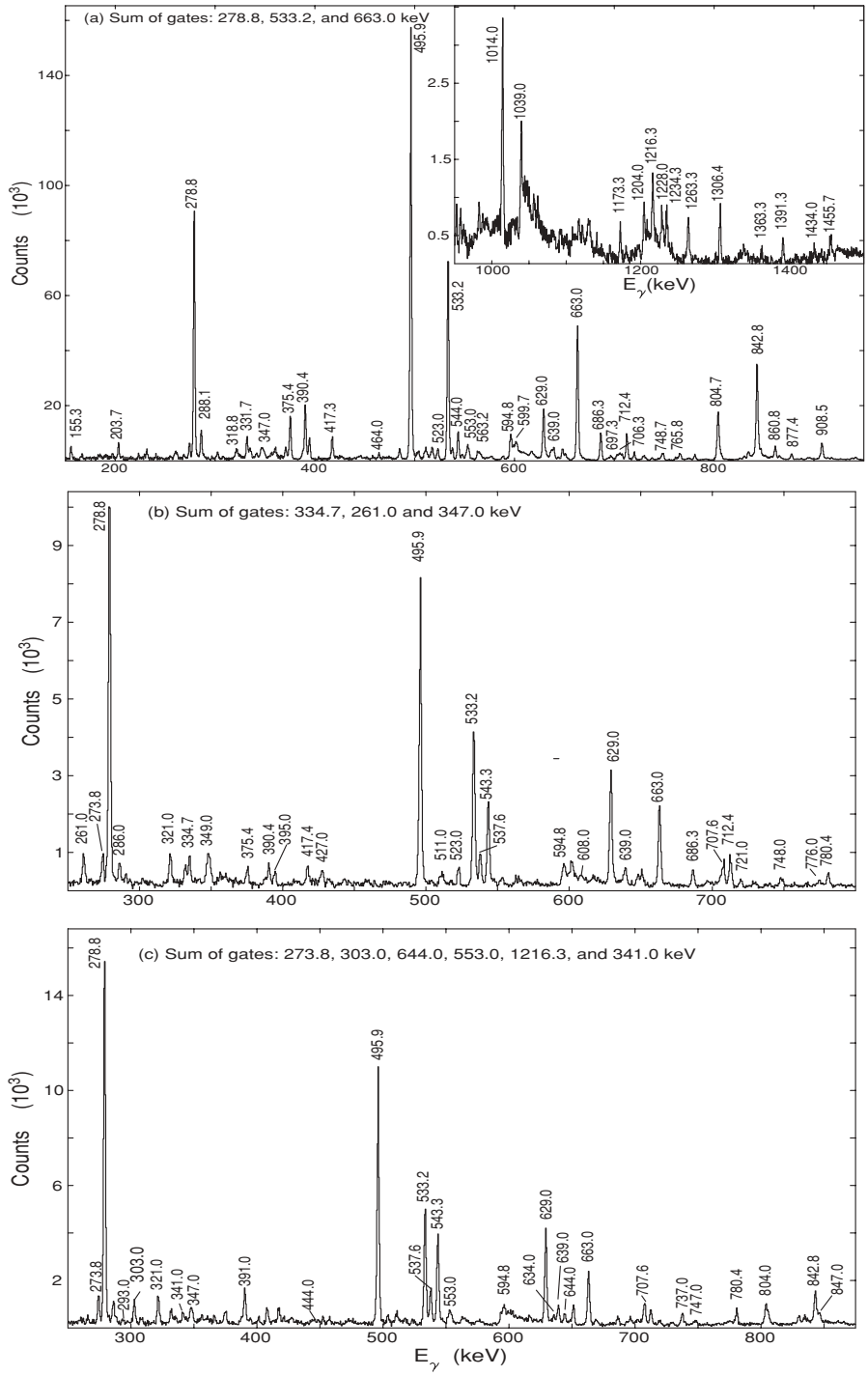

FIG. 5. γ-ray summed coincidence spectra with gates on the mentioned transitions depicting γ transitions related mainly to negative-parity bands (a) B9 and B15, (b) B13, and (c) B14.

give rise to its isomeric nature causing difficulty in fixing the decaying transitions from this bandhead.

B. Negative-parity bands

1. B10 band

The negative-parity sequence built on the $11/2^-$ state is the favored signature ($\alpha = -1/2$) partner in the $\pi h_{11/2}$ band (B10). The favored signature partner has relatively large intensity, whereas the unfavored signature ($\alpha = +1/2$) partner has a weakly populated sequence comprising the 616.8, 637.6, and 860.8 keV transitions. In the present experiment, the 372.0, 619.1, and 761.3 keV $E1$ transitions have been observed between the states of the $\pi d_{5/2}$ (B6) and $\pi h_{11/2}$ (B10) bands [Fig. 4(b)].

2. B9 and B15 bands

The γ-vibrational band built on the favored signature partner of the $\pi h_{11/2}$ band, a feature observed in the ^{123,125,127}Cs isotopes [29–31], was not observed in the heavier ^{129,131,133}Cs

isotopes [23,24,32] prior to this work. The B9 band observed in the present work is likely to be the γ-vibrational band coupled to the $\pi h_{11/2}$. This band is built on the 2007 keV ($I^\pi = 15/2^-$) level and has been observed up to the 4044 keV ($I^\pi = 27/2^-$) level. This band is feeding the $\pi h_{11/2}$ band (B10) through strong 1231.1, 1263.3, 1306.4, and 1228.0 keV $E2$ transitions. In addition, there are interband 318.8, 464.0, 599.7, and 697.3 keV $M1/E2$ transitions from B9 band to B10 band.

B15 band has also been observed for the first time in the present work. The strongest out feeding is through the 1391.3 keV transition from the lowest observed 2701 keV level ($I^\pi = 19/2^-$) of B15 to the $15/2^-$ level of the B10 band ($\pi h_{11/2}$). Higher levels in B15 also decay to the corresponding levels of B10. In this respect, the B15 band seems to have a structure similar to B9. The gated spectrum showing the transitions of bands B9 and B15 is depicted in Fig. 5(a).

3. B11 band

The B11 band has been substantially extended up to the 6202 keV ($I^\pi = 39/2^-$) level. There are two cascades 554.2–348.0 keV and 485.8–516.0 keV of dipole transitions which feed the $29/2^-$ and $31/2^-$ levels of the B11 band, respectively. A 341.0 keV $M1$ transition also feeds to the $33/2^-$ level of the B11 band.

4. B12 band

The previously established coupled negative-parity band B12 is also extended up to the 4719 keV ($I^\pi = 31/2^-$) level. This band decays to the favored partner of the $\pi h_{11/2}$ band through the 993.7, 1057.2, 1091.6, and 1173.3 keV $E2$ transitions and to the unfavored partner of the $\pi h_{11/2}$ band through the 352.2, 404.5, and 321.5 keV $M1$ transitions. The multipolarities of these transitions have been established from DCO ratios. This band is also fed by the 1048.0, 983.0, and 958.0 keV $E2$ transitions at the $29/2^-, 27/2^-$ and $25/2^-$ states, respectively. The negative-parity coupled B11 band feeds the B12 band through the 400.1 keV ($25/2^- \rightarrow 23/2^-$) $M1$ transition.

5. B13 band

The B13 band is reported for the first time and is observed up to $I^\pi = 25/2^-$. The strongest decay out from the band is via the 1234.3 keV transition to the $15/2^-$ level of the $\pi h_{11/2}$ (B10) band. The measured DCO ratio of 1.25 for the 1234.3 keV transition suggests its $E2$ multipolarity. Several $E2$ and $M1$ transitions from levels of the B13 band feed levels in B12. There are decaying transitions from the lowest observed 2284 keV level of band B13 to the $15/2^-$ member of band B12, together with similar decay from the higher members of this band to the corresponding members of band B12. The measured DCO ratio of 0.62 for the 334.7 keV transition to the $15/2^-$ member of the B12 band determines the spin $I^\pi = 17/2^-$ for the 2284 keV bandhead of the B13 band. These interband transitions favored negative parity for the B13 band, the same as that of B12. The gated spectrum for this band is shown in Fig. 5(b).

6. B14 band

Observed for the first time in this study, the negative-parity coupled band B14 has the bandhead at the 2223 keV ($I^\pi = 17/2^-$) level and has been further extended up to the 5005 keV ($I^\pi = 31/2^-$) level. The spin-parity assignments for this band are based on the measured DCO ratio of 0.85 for the 1216.3 keV transition to the $15/2^-$ member of the negative-parity $\pi h_{11/2}$ (B10) band suggesting an $E2$ multipolarity. There is an 898.3 keV transition from the bottom of B14 that is feeding to the 1325 keV ($I^\pi = 15/2^+$) level of B5. The 2526 keV level ($I^\pi = 19/2^-$) of B14 feeds the $15/2^-$ level in B12 with the 576.8 keV transition, and the 552.3 keV transition feeds to the $19/2^-$ state of B10. The gated spectrum for this band is shown in Fig. 5(c). The bandhead 2223 keV ($I^\pi = 17/2^-$) of B14 and the level 2223 keV ($I^\pi = 17/2^-$) of B12 have nearly the same energy.

IV. THEORETICAL MODELS

Projected Hartree-Fock (PHF) calculations have been carried out to assign the microscopic structures of most of the observed bands in ^{131}Cs. The basic outline of the PHF model is described in the following subsection. The tilted-axis cranking (TAC) model has been used to describe the nearly degenerate bands B2 and B3. The strongly coupled band B2 has been reassigned a high-K three-quasiparticle configuration based on TAC and PHF calculations along with the systematics of similar bands in nearby nuclei. The TAC model is well described in Refs. [8,33,34] and has been also used to describe dipole bands in nuclei with A $\sim$130 [13].

A. Projected Hartree-Fock (PHF) calculations

PHF is a powerful microscopic model for studying the spectroscopic properties of high spin states in well-deformed and moderately deformed nuclei. This model gives the quantum mechanical description of the collective rotation and its coupling with single-particle excitations in a self-consistent basis. Microscopic descriptions of bands in ^{131}Cs have been obtained with the help of PHF calculations. The measured energy levels and the ratio of the electromagnetic transition strengths are compared with the calculated ones. The deformed HF equation is derived from the nuclear Hamiltonian that consists of the single-particle and two-body interaction terms [35,36]. The surface delta interaction with strength $V_{pp} = V_{np} = V_{nn} = 0.34$ MeV is taken as two-body residual interaction among the active nucleons. The spherical single-particle states used for PHF calculations are $3s_{1/2}, 2d_{3/2}, 2d_{5/2}, 1g_{7/2}, 1g_{9/2}, 1h_{9/2}$, and $1h_{11/2}$ with energies 3.654, 3.288, 0.0, 0.64, -6.541, 5.033, and 0.8 MeV, respectively, for protons and $3s_{1/2}, 2d_{3/2}, 2d_{5/2}, 1g_{7/2}, 2f_{7/2}, 1h_{9/2}$, and $1h_{11/2}$ with energies -4.848, -4.577, -6.4, -6.0, 1.592, 2.106, and -3.2 MeV, respectively, for neutrons. The model space considered here is

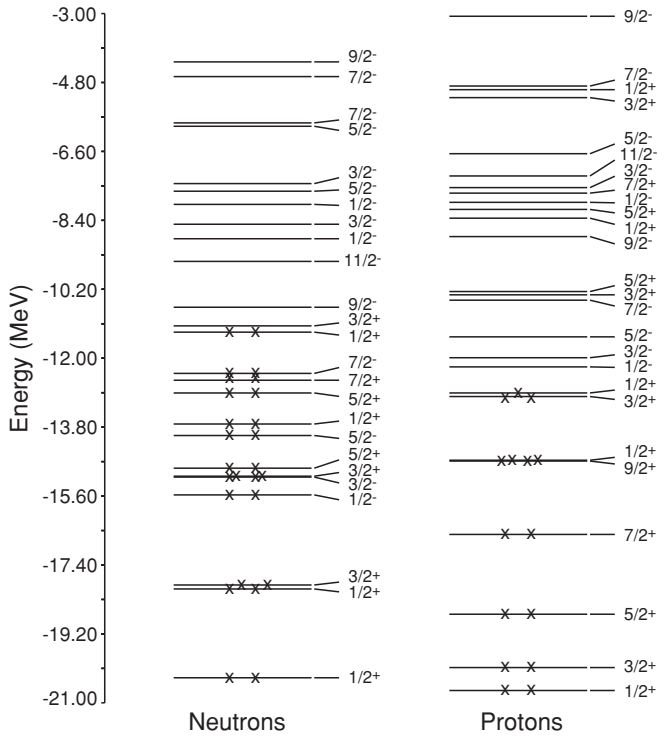

FIG. 6. Prolate deformed Hartree-Fock orbits for neutrons and protons.

outside the inert spherical core with $Z = 40$ and $N = 50$. HF iteration is performed for both prolate and oblate deformations. The prolate HF mean field solution is energetically favored for ^{131}Cs giving the deformation as $\beta = 0.21$ (effective charges $1.7e$ and $0.7e$ are taken for protons and neutrons, respectively). Axial symmetry of the Hartree-Fock field is assumed in the calculation. The prolate Hartree-Fock orbits for ^{131}Cs are plotted in Fig. 6. One can get an intrinsic state $|\phi_K\rangle$ by making appropriate particle-hole arrangements on deformed HF orbits near the proton and neutron Fermi surfaces. For one-quasiparticle bands, the odd proton occupies a particular orbit, and the rest of the active nucleons (14 protons and 26 neutrons) fill the lowest time-reversal symmetric proton and neutron orbits. The given intrinsic state $|\phi_K\rangle$ does not have a unique angular momentum quantum number I and is a superposition of various I states (intrinsic states are states of good K but not of good I).

$$|\phi_K\rangle = \sum_I C_K^I |\Psi_K^I\rangle. \tag{1}$$

To study the band structure and electromagnetic matrix elements we need good angular momentum states ($|\Psi_K^I\rangle$); these good I states are obtained by angular momentum projection from $|\phi_K\rangle$. The I projection operator is [37]

$$P_K^{IM} = \frac{2I+1}{8\pi^2} \int d\Omega D_{MK}^{I^*}(\Omega) R(\Omega), \tag{2}$$

where R(Ω) is the rotation operator.

The matrix element of the Hamiltonian between projected states of I obtained from intrinsic states $|\phi_{K_1}\rangle$ and $|\phi_{K_2}\rangle$ is

$$H_{K_1K_2}^I = \frac{2I+1}{2} \frac{1}{\left(N_{K_1K_1}^I N_{K_2K_2}^I\right)^{1/2}} \times \int_0^\pi d\beta \sin(\beta) d_{K_1K_2}^I(\beta) \langle\phi_{K_1}| H e^{-i\beta I_y} |\phi_{K_2}\rangle. \tag{3}$$

Here

$$N_{K_1K_2}^I = \frac{2I+1}{2} \int_0^\pi d\beta \sin(\beta) d_{K_1K_2}^I(\beta) \langle\phi_{K_1}| e^{-i\beta I_y} |\phi_{K_2}\rangle \tag{4}$$

has been found to be the amplitude overlap for angular momentum I.

In general, two states $|\Psi_{K_1}^{IM}\rangle$ and $|\Psi_{K_2}^{IM}\rangle$ projected from two intrinsic states $|\phi_{K_1}\rangle$ and $|\phi_{K_2}\rangle$ are not orthogonal to each other even if intrinsic states are orthogonal. For the band mixing calculation, we orthonormalize them and then diagonalize using the equation

$$\sum_{K'} \left(H_{KK'}^I - E_I N_{KK'}^I\right) C_{K'}^I = 0, \tag{5}$$

where $C_{K'}^I$ is the orthonormalized amplitude, which is also known as the band-mixing amplitude. More details of this formalism can be found in Refs. [35,36,38].

V. DISCUSSION

The level scheme of ^{131}Cs shows properties typical of rotational deformed nuclei. The different bands observed in this nucleus are mainly based on one- or three-quasiparticle configurations. The experimentally determined spins and level energies have been transformed into the rotating frame of reference following the prescription of Bengtsson and Frauendorf [39]. The Harris parameters [40] $J_0 = 5.8\hbar^2$ MeV^{-1} and $J_1 = 50.8\hbar^4$ MeV^{-3} have been used. The Routhian (e') and alignment (i_x) extracted for these bands are shown as a function of rotational frequency in Fig. 7. It is seen that single-proton bands B5 ($\pi g_{7/2}$) and B6 ($\pi d_{5/2}$) show alignments $\sim 2\hbar$, whereas band B10 ($\pi h_{11/2}$) shows an alignment $\sim 5\hbar$. The excited bands B2, B3, B7, B8, B11, B12, B13, and B14 exhibit alignments $\geqslant 6\hbar$, indicating three-quasiparticle configurations involving contributions from high-j orbitals. In addition, the B8 band shows an upbend at $\hbar\omega \sim 0.5$ MeV, suggesting a five-quasiparticle configuration after the upbend. Routhians of bands B11–B14, are nearly parallel and higher than that of B10. This also suggests the contribution from the high-j shape driving the $\pi h_{11/2}$ orbital to the B11–B14 bands. Suitable configurations have been assigned to these bands on the basis of the above observations and the comparison of the PHF calculations based on these configurations with the experimental energy levels and $B(M1)/B(E2)$ ratios. A systematic discussion of different bands observed in ^{131}Cs is given below.

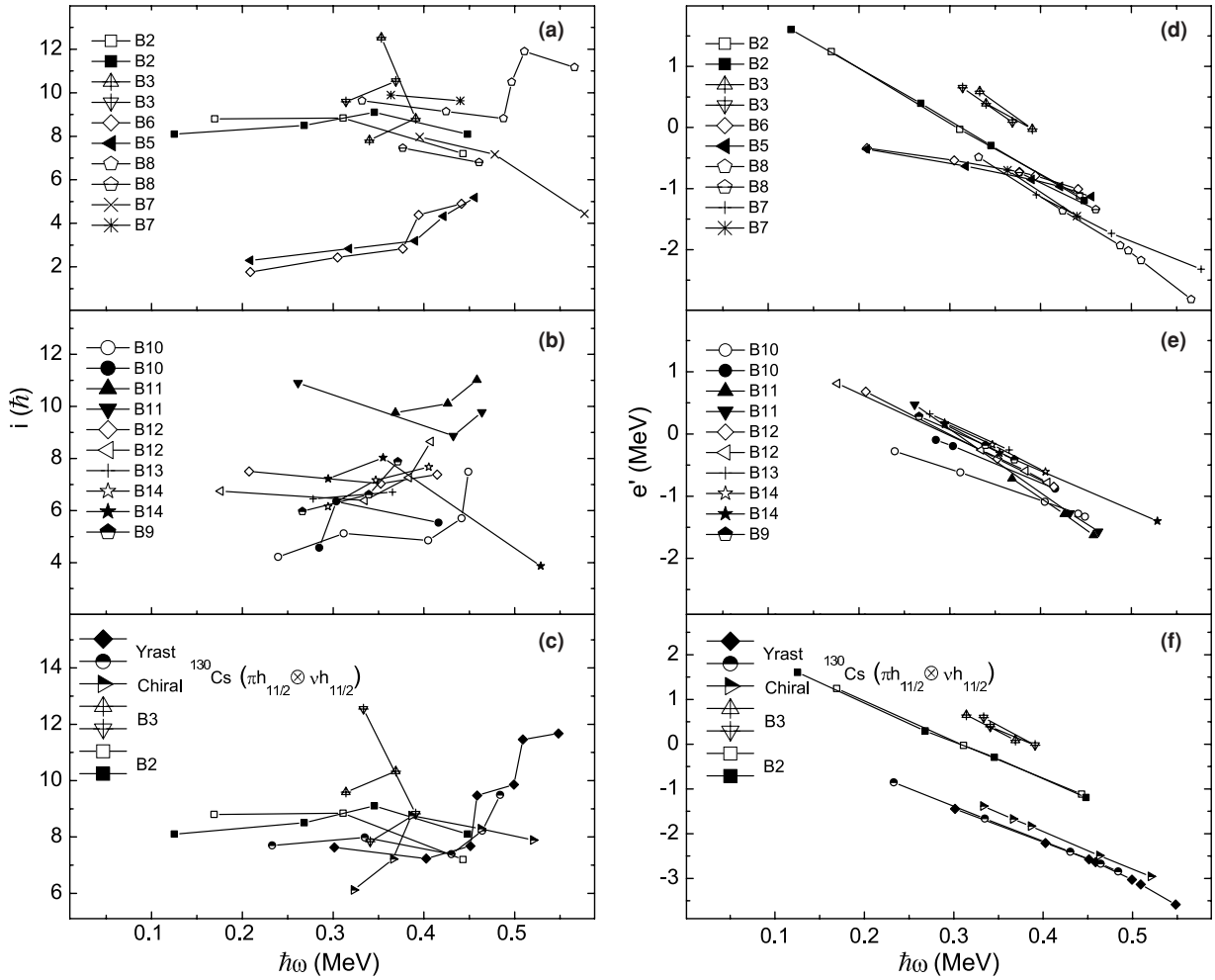

FIG. 7. Alignment plots (a) and (b), and the Routhian plots (d) and (e) for different positive and negative-parity bands in ^{131}Cs. Alignment and Routhian plots for twin chiral bands in ^{130}Cs are compared with those of bands B2 and B3 in ^{131}Cs in (c) and (f).

A. Positive-parity quasiparticle bands

1. B5 and B6 bands

The experimental bands B5 and B6 are compared with one-quasiproton configurations based on $\Omega = 3/2^+$ and $\Omega = 1/2^+$ orbits, respectively (these orbits are mainly of $g_{7/2}$ and $d_{5/2}$ origin). The above quasiproton bands are mixed with $\Delta K = 1$ rotational aligned (RAL) bands to obtain better agreement of level spacings at higher spins. We have performed three-by-three band mixing in both cases and compared the lowest states after the band mixing with the experimentally observed band. The first RAL band is obtained by exciting one neutron from the $\Omega = 7/2^-$ to the $\Omega = 9/2^-$ orbit; while the second RAL band is obtained by exciting one neutron from the $\Omega = 1/2^+$ to the $\Omega = 3/2^+$ orbit. The theoretical results are compared with experimental data in Fig. 8 and found to be in good agreement. For comparison of the observed relative level spacings with calculation, the $I^\pi = 5/2^+$ state is normalized for B6. Similarly, normalization is done for the $I^\pi = 7/2^+$ state of band B5. Experimentally, the unfavored branches of these bands have not been observed. This may be because of the large signature splitting present in these two bands originated from low-Ω and high-j configurations.

2. B2 and B3 bands

The two positive-parity coupled bands, namely, B2 and B3 based on the $17/2^+$ and $25/2^+$ states, respectively, are seen. The new band B3 is observed to decay only to band B2. Band B2 decays with most of the interband transitions to band B6 and a few to B5. The plots of level energies E vs angular momentum I for bands B2 and B3, shown in the Fig. 9(a), exhibit a close resemblance to a small energy difference ranging from ~50 to 250 keV. It is remarkable to have such a small energy difference over a wide observed spin range and at high excitation energy. Band B3 at all the observed levels decays into the corresponding states of band B2 through $\Delta I = 1$ and $\Delta I = 2$ transitions. In addition, the experimental $B(M1)/B(E2)$ ratios for the intraband transitions of the two bands agree within experimental errors. It is evocative that both these bands are based on nearly similar configurations. In the earlier work by Kumar *et al.* [24], a three-quasiparticle

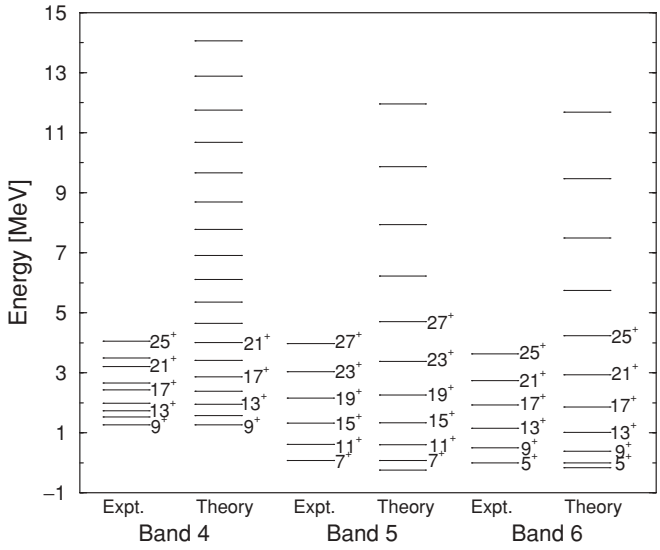

FIG. 8. Comparison of the experimental positive-parity levels in bands B4, B5, and B6 with results of the microscopic deformed Hartree-Fock model after normalization of bandhead energies (see text). $2I$ is indicated as the spin of various levels.

configuration $\pi g_{7/2}/d_{5/2} \otimes (\nu h_{11/2})^2$ was assigned to band B2. In this scenario, the band B3 can be thought of as having a large overlap in configuration with that of band B2, and one of the most probable configurations for band B3 would be $\pi g_{7/2}/d_{5/2} \otimes (\pi h_{11/2})^2 \otimes (\nu h_{11/2})^2$. However, the alignment plot [Fig. 7(a)] for the observed portion of band B3 is not adequate to conclude the possibility of accommodating five high aligned quasiparticles. Also, the $(\nu h_{11/2})^2$ pair alignment occurs at ∼0.5 MeV in band B8 [see Fig. 7(a)], and the above-mentioned five-quasiparticle configuration is a better fit for the upper portion of band B8. Therefore, it is not possible to explain the two similar coupled band structures B2 and B3 on the basis of the earlier assigned $\pi g_{7/2}/d_{5/2} \otimes (\nu h_{11/2})^2$ configuration [24], and other alternatives need to be explored.

Recently, a similar pair of coupled band structures involving the $\pi h_{11/2} \otimes \nu h_{11/2} \otimes \nu g_{7/2}$ configuration have been observed in ^{125}Cs [29] and a single coupled band structure in ^{129}Cs [41]. Similarity of plots of level energy E vs angular momentum I, as shown in Fig. 9(a), favors the involvement of the $\pi h_{11/2} \otimes \nu h_{11/2}$ component in the configuration of bands B2 and B3. This is the yrast configuration in the neighboring odd-odd ^{126,128,130}Cs [42–44] isotopes. The excited chiral partners based on this configuration have also been observed in these isotopes.

The Routhian and alignment for the B2 and B3 bands are included in Figs. 7(c) and 7(f) along with the $\pi h_{11/2} \otimes \nu h_{11/2}$ yrast and chiral bands of ^{130}Cs. The alignment gain closely matches that for the yrast band in ^{130}Cs, indicating that the third quasiparticle has to be a positive-parity orbital $d_{3/2}$ or $s_{1/2}$ with low alignment gain. The Routhians for both bands B2 and B3 are parallel to the yrast band in ^{130}Cs. These points favor the configurations with the $\pi h_{11/2} \otimes \nu h_{11/2}$ component. The TAC model calculations have been performed for all possible three-quasiparticle configurations on the basis of Nilsson diagrams leading to positive-parity bands.

The configuration $\pi h_{11/2} \otimes \nu h_{11/2} \otimes \nu d_{3/2}$ reproduces the bandhead angular momentum. A self-consistent TAC calculation with this choice of configuration has resulted in the deformation parameters $\epsilon_2 = 0.122$, $\epsilon_4 = 0.0$, $\gamma = 30^\circ$, and an average tilt angle $\theta = 57^\circ$ for the angular momentum with the principal axis. The resulting angular momentum (I) vs rotational frequency ($\hbar\omega$) plot shown in Fig. 10 exhibits remarkable agreement with the experimental plot. Furthermore, the calculated $B(E2)$ values are also extremely small. The $E2$ crossover transitions are not observed at the

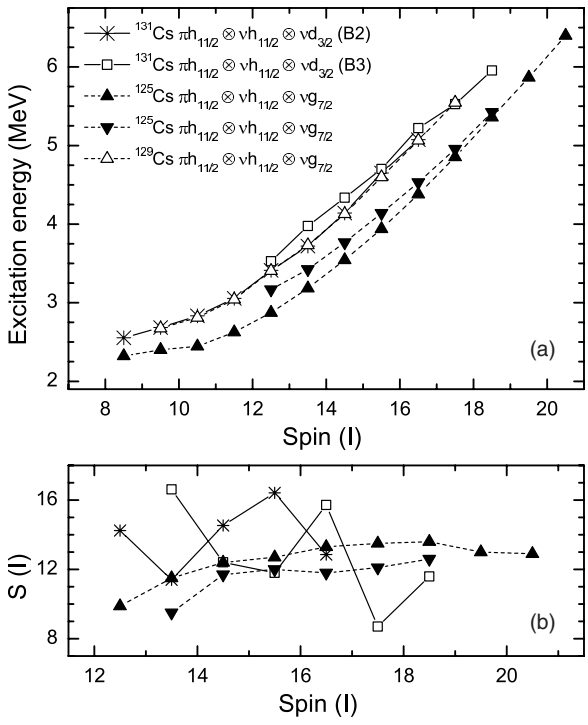

FIG. 9. (a) Excitation energies of levels in bands B2 and B3 of ^{131}Cs along with those of bands with configurations involving $\pi h_{11/2} \otimes \nu h_{11/2}$ in ^{125,129}Cs. (b) Energy staggering in bands B2 and B3 of ^{131}Cs compared with that of bands with configurations involving $\pi h_{11/2} \otimes \nu h_{11/2}$ of ^{125}Cs.

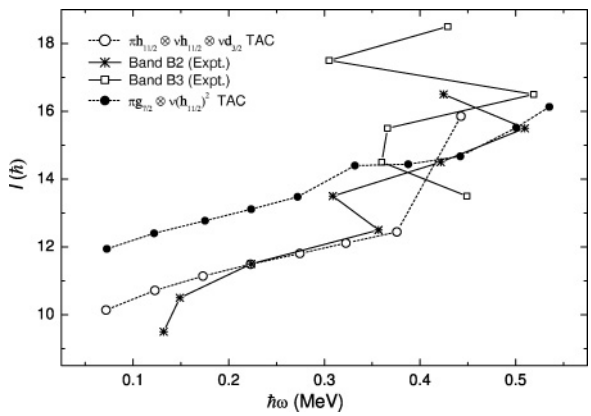

FIG. 10. Spin (I) vs frequency ($\hbar\omega$) plots of B2 and B3 bands. The TAC calculations based on different configurations are shown for comparison.

lower levels and appear at higher frequencies. The calculated ratios of transition probabilities, $B(M1)/B(E2)$, are quite large in this region. These considerations support the $\pi h_{11/2} \otimes \nu h_{11/2} \otimes \nu d_{3/2}$ configuration for the B2 band.

The self-consistent TAC calculation has also been performed for the three-quasiparticle configuration $\pi g_{7/2}/d_{5/2} \otimes \nu(h_{11/2})^2$. This gives the deformation parameters $\epsilon_2 = 0.111$, $\epsilon_4 = 0.0$, $\gamma = 46^\circ$, and an average tilt angle $\theta = 16^\circ$. The result of the calculations of angular momentum (I) vs rotational frequency ($\hbar\omega$) plot is also shown in the Fig. 10. It is seen that the overall agreement of the TAC calculations with the experimental data is better for the $\pi h_{11/2} \otimes \nu h_{11/2} \otimes \nu d_{3/2}$ configuration than for the $\pi g_{7/2}/d_{5/2} \otimes \nu(h_{11/2})^2$ configuration. The B2 and B3 bands are, therefore, likely to be built on the three-quasiparticle $\pi h_{11/2} \otimes \nu h_{11/2} \otimes \nu d_{3/2}$ configuration. The $E(I)$ vs I plot in Fig. 9(a) shows that B2 and B3 bands are nearly degenerate in energy. Both B2 and B3 show zig-zag behavior in the staggering $S(I)$ vs I plot. The $B(M1)/B(E2)$ values for these bands are also similar, as shown in Fig. 12. Therefore, the B2 and B3 bands can be assigned a $\pi h_{11/2} \otimes \nu h_{11/2}$ configuration responsible for the chirality in odd-odd Cs isotopes, coupled with a $d_{3/2}$ quasineutron, which acts as a spectator. Degenerate bands based on similar configurations have been observed in odd-A ^{125}Cs [29].

Further, state-of-the-art PHF calculations are also carried out to understand the microscopic structure of these two nearly degenerate bands. For these bands, we have considered two different sets of configurations and performed an angular momentum projection. In the first set of configurations, we considered the odd proton in $d_{5/2}$ or $g_{7/2}$ and the two unpaired neutrons in $h_{11/2}$ orbits with $K = 17/2^+$ and $K = 19/2^+$. In the second set, we considered the odd proton in $h_{11/2}$ and the two odd neutrons in $d_{3/2}$ and $h_{11/2}$ with $K = 13/2^+$ and $K = 15/2^+$. In the first set, the theoretical level spacings are larger than the corresponding experimental level spacings (see Fig. 11). In the second case, the agreement of level spacings

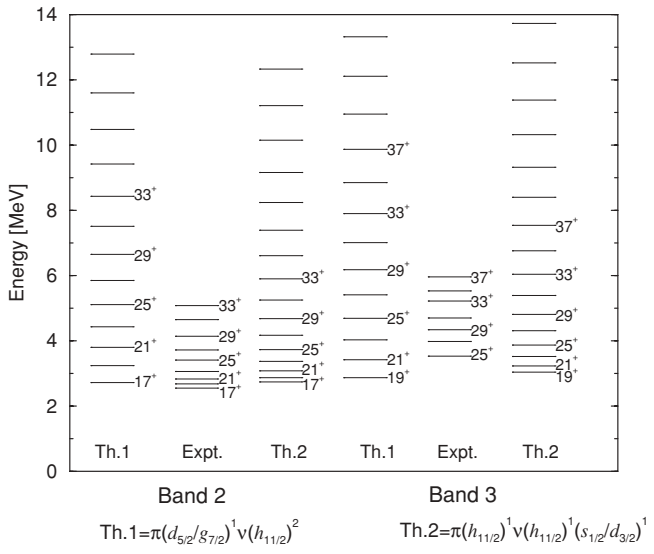

FIG. 11. Comparison of experimental levels in bands B2 and B3 with the results of the microscopic deformed Hartree-Fock model. $2I$ is indicated as the spin of various levels.

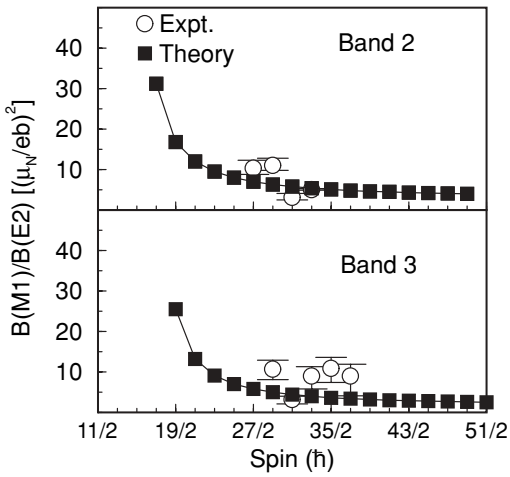

FIG. 12. Comparison of measured $B(M1)/B(E2)$ ratios for transitions in bands B2 and B3 with results of microscopic deformed Hartree-Fock model based on configurations given in set II.

is much better. However, this configuration (set II) is unable to explain the absence of the observed transitions to band B10. The measured $B(M1)/B(E2)$ ratios are compared with calculations [36] based on set II in Fig. 12. Similarly, for set I, the $B(M1)/B(E2)$ ratios were extracted. It has qualitatively the same trend with spin as that of set II, while the absolute values are found to be about twice those in set II. After the comparison of the experimental energy spectra and ratio of transition strengths with the calculations, the overall agreement is better for configurations based on set II. Therefore, the high-K configurations mentioned as set II may be more appropriate for B2 and B3 bands as per the PHF calculations.

$$K = 17/2^+, \quad \pi 1/2^+(d_{5/2})\nu(7/2^- + 9/2^-)(h_{11/2}) \text{ (set I)},$$
$$K = 19/2^+, \quad \pi 3/2^+(g_{7/2})\nu(7/2^- + 9/2^-)(h_{11/2}) \text{ (set I)},$$
$$K = 13/2^+, \quad \pi 1/2^-(h_{11/2})\nu 3/2^+(d_{3/2})9/2^-(h_{11/2}) \text{ (set II)},$$
$$K = 15/2^+, \quad \pi 3/2^-(h_{11/2})\nu 3/2^+(d_{3/2})9/2^-(h_{11/2}) \text{ (set II)}.$$

3. B7 and B8

Multiquasiparticle bands B7 and B8 are built above bands B5 and B6, respectively. These bands are explained in the PHF calculations by considering three-quasiproton configurations with $\pi(h_{11/2})^2$ coupled to $\pi g_{7/2}$ or $\pi d_{5/2}$. Looking into the alignment plot for band B8 in Fig. 7(a), the five-quasiparticle RAL band based on $\pi d_{5/2} \otimes \pi(h_{11/2})^2 \otimes \nu(h_{11/2})^2$ has been mixed with the above three-quasiproton configuration. Experimentally, both signature partner branches have been observed with small staggering among them. The PHF calculations also give the proper signature splitting between favored and unfavored branches. Comparison of the theoretical and experimental spectra of these two bands is shown in Fig. 13. The $I^\pi = 27/2^+$ and $I^\pi = 21/2^+$ states of bands B7 and B8, respectively, are normalized to the experimental energies. After the alignment, calculations indicated a slight increase in deformation due to occupation of $h_{11/2}$ orbitals.

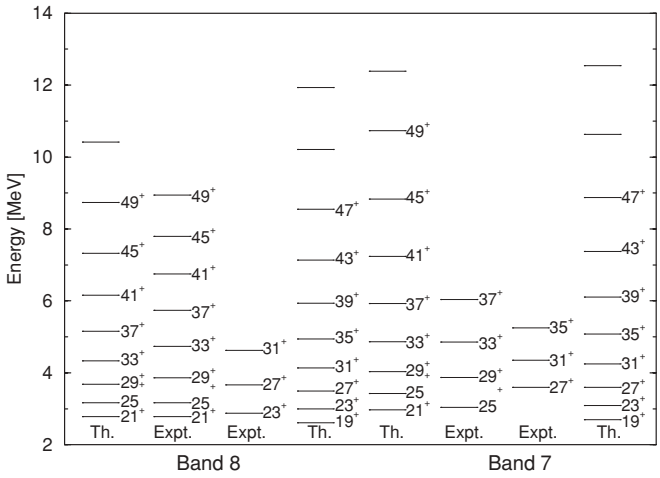

FIG. 13. Comparison of experimental levels in bands B7 and B8 with results of microscopic deformed Hartree-Fock model. $2I$ is indicated as the spin of various levels. For band B8, the $I = 21/2^+$ state is normalized; for band B7, $I = 27/2^+$ is normalized.

4. B4 band

The other tentatively assigned positive-parity band B4 is compared with a one-quasiproton band obtained by considering the proton hole in the $g_{9/2}$ orbital with $K = 9/2$. RAL band mixing has been carried out for this band, and the band mixing spectrum is compared with the experimental spectrum in Fig. 8. The RAL bands are obtained by exciting one neutron from the $\Omega = 7/2^-$ to the $\Omega = 9/2^-$ orbit, while the second RAL is obtained by exciting one neutron from $\Omega = 1/2^+$ to $\Omega = 3/2^+$ orbit. As the experimental excitation energy of $I = 9/2$ state is not known, it is normalized with the calculated bandhead for comparison of energy levels of other states in this figure. Interestingly, the calculated bandhead is around 1.2 MeV excitation energy with respect to the $I^\pi = 5/2^+$ state of band B6 ($\pi d_{5/2}$), which is very close to the prediction of the systematics as discussed in the previous section. We found the agreement is reasonable. This quasiproton band naturally emerges from the PHF calculations, and thus it will be worthwhile to search for a similar band structure in nearby Cs isotopes.

B. Negative-parity quasiparticle bands

1. B10 band

The low-lying negative-parity band B10 has been compared with the one-quasiproton negative-parity band. This band is obtained by exciting the odd proton to the $\Omega = 1/2^-$ orbit of $h_{11/2}$ followed by angular momentum projection. Two other bands, obtained by exciting the odd proton to $\Omega = 3/2^-$ and $\Omega = 5/2^-$ orbits of $h_{11/2}$, have also been mixed with the above band built on the $\Omega = 1/2^-$ orbit, for obtaining better signature splitting and level spacings. The calculations showed reasonable agreement with the experimental observations, as shown in Fig. 14.

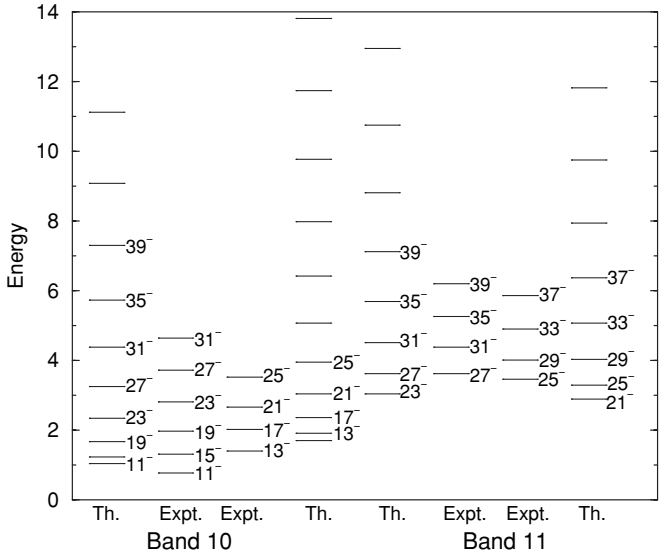

FIG. 14. Comparison of experimental levels in bands B10 and B11 with results of microscopic deformed Hartree-Fock model. $2I$ is indicated as the spins for the different states. $27/2$ state is normalized to the experimental energies of levels of B11.

2. B11 band

The three-quasiparticle negative-parity band B11 is built above band B10. The signature splitting of B11 is found to be smaller than that of B10, suggesting configurations with large K values. Therefore, the three-quasiparticle configuration $\pi(h_{11/2})^1 \otimes \nu(7/2^- + 9/2^-)(h_{11/2})$ with $K = 17/2^-$ has been used for the angular momentum projection calculation. The calculated energy spectrum is compared with the experimental data in Fig. 14 and found to be in fair agreement. The measured ratio of $B(M1)/B(E2)$ transition strengths vary between 5 and 10 $\mu_N^2/(e\text{b})^2$.

3. B12 and B13 bands

Interband transitions from B12 and B13 bands to B10 have been observed in the present experiment. Therefore, different three-quasiparticle configurations with an odd proton in $h_{11/2}$ have been considered for angular momentum projection. One of the two neutrons is kept in the $\Omega = 7/2^+$ orbit (based on $g_{7/2}$). The other neutron is placed in the $\Omega = 3/2^+$ orbit (based on $d_{3/2}$) for one band and in the $\Omega = 1/2^+$ orbit (based on $s_{1/2}$) for the other band. The calculated energy level spectra and the $B(M1)/B(E2)$ ratios for B12 and B13 are plotted against the experimental data in Figs. 15 and 16 for comparison. The calculations are in reasonable agreement with experimental observations.

4. B14 band

It has been observed that the lower levels of band B14 decay to both B5 and B10 bands. This suggests that the configuration of this band may have both B5 and B10 components. Based on this observation, following three quasiproton configurations

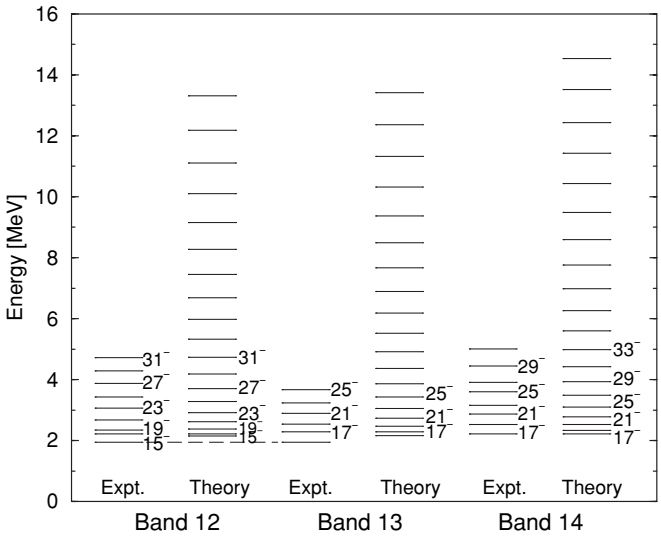

FIG. 15. Comparison of experimental levels in bands B12, B13 and B14 with results of microscopic deformed Hartree-Fock model. $2I$ are indicated as the spin of various levels. Theoretical $I = 17/2^-$ states are normalized to the observed states in each of these bands.

have been considered for the angular momentum projection:

$$\pi 9/2^+(g_{9/2})1/2^+(d_{5/2})1/2^-(h_{11/2})$$

and

$$\pi 9/2^+(g_{9/2})3/2^+(g_{7/2})1/2^-(h_{11/2}).$$

When these two configurations are diagonalised after angular momentum projection, the later configuration is found to have maximum component for B14.

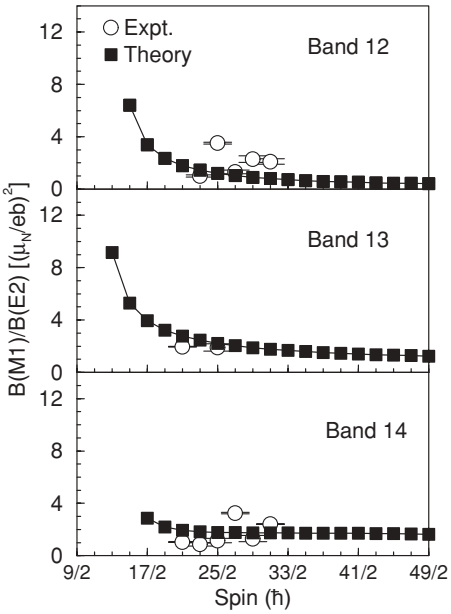

FIG. 16. Comparison of measured B(M1)/B(E2) ratio for transitions in band B12, B13, and B14 with results of microscopic deformed Hartree-Fock model.

Fig. 15 and Fig. 16 show good agreement of the measured energy levels and the B(M1)/B(E2) ratios with the calculations for the B14 band.

C. Gamma vibrational bands

The energy level spacings (staggering pattern) and transition strengths of γ-vibrational bands provide information regarding the triaxiality of the even-even nuclei in the A $\sim$130 mass region [5]. In the present work, two bands, namely, B1 and B9, have been observed for the first time. The decay pattern of band B9, with bandhead spin of $I^\pi = 15/2^-$, is found to be quite similar to that of the γ-vibrational band built on the favored signature of the $\pi h_{11/2}$ band in lighter Cs isotopes [29,31]. It will be interesting to experimentally identify the states of the γ-vibrational band with intermediate spins $I^\pi = 17/2^-, 21/2^-$, etc. The excited states of B1 decay to the band B5 via the $\Delta I = 1$ transitions with energy higher than 1 MeV. Thus, B1 has been identified as the γ band coupled with the $\pi g_{7/2}$ orbital. Similar band structure has not been observed in neighboring odd Cs isotopes. The bandhead of the γ band coupled with $\pi g_{7/2}$ orbital is expected to be $I^\pi = 11/2^+$. However, the lowest energy state observed in B1 has a spin $I^\pi = 13/2^+$. For comparison of the relative level spacings of B1 and B9 with that of the γ band of neighboring even-even nucleus ^{130}Xe [45], the $13/2^+$ state of band B1 and $15/2^+$ state of band B9 have been normalized to 3^+ and 2^+ states of that in ^{130}Xe, respectively (see Fig. 17). The γ band B1 built on $\pi g_{7/2}$ seems to have the same staggering pattern as that of ^{130}Xe. At present, a similar comparison for B9 is not possible as the intermediate levels have not yet been identified. Another negative-parity band, B15, has been found in the present work, which has a level spacing and feeding pattern similar to the favored signature of the $\pi h_{11/2}$ band as that of B9. Though an equivalent band has been identified in

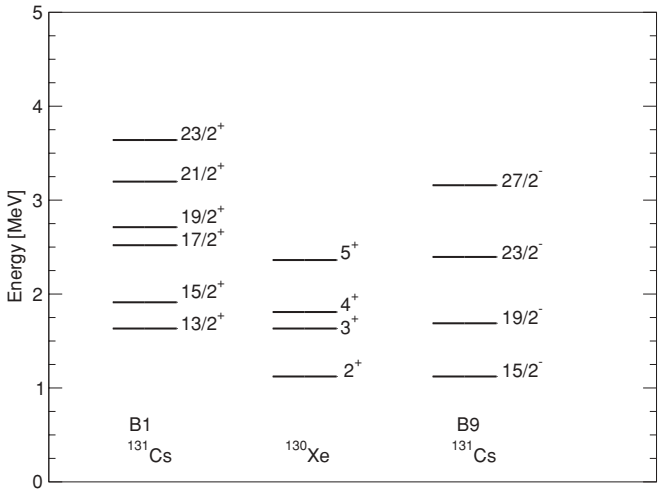

FIG. 17. Comparison of the relative spacing of the experimental levels in gamma bands B1 and B9 of ^{131}Cs with that of neighboring ^{130}Xe nucleus. Spins of the different states are marked for each band. The lowest observed states of all these gamma bands are normalized as explained in the text.

^{125}Cs [29], more experimental data in other odd Cs isotopes along with theoretical calculations are required to identify the microscopic structure of the B15 type band. It is important to note that through such systematic comparison of the structures of γ bands coupled with different quasiparticles in even-odd and odd-even nuclei (e.g., ^{131}Cs), one can understand the coupling of the high-j particles to the even-even triaxial core (e.g., ^{130}Xe). This interesting aspect in return would shed more light on such a phenomenon as chiral doublet bands in odd-odd nuclei (e.g., ^{132}Cs) which arises from the coupling of a triaxial even-even core with high-j particle and hole.

D. Octupole collectivity in ^{131}Cs

Neutron-deficient isotopes around $Z = 54$ are predicted to show a softness with respect to octupole deformation at low spin. The signature for such effects are interleaved positive- and negative-parity bands connected by enhanced $E1$ transitions. This is because both proton and neutron levels, arising from the same $h_{11/2}$ and $d_{5/2}$ orbitals ($\pi = -1$, $\Delta l = \Delta j = 3$), are near the Fermi surface. The $\pi h_{11/2}$, $\pi d_{5/2}$, and $\pi g_{7/2}$ bands are seen in the odd-A $^{117,121-133}$Cs isotopes. The population strength of the $\pi g_{7/2}$ and $\pi d_{5/2}$ bands relative to that of the $\pi h_{11/2}$ band increases considerably with increasing mass number. This happens primarily because the excitation energy of the $h_{11/2}$ orbital is increasing thus becoming less yrast in the heavier isotopes. These facts are consistent with a decreasing nuclear deformation with increasing mass. Also, in the lighter Cs and I isotopes, significant admixture of $\pi d_{5/2}$ orbitals has been noticed in the $\pi g_{7/2}$ bands. Features of the $\pi g_{7/2}$ and $\pi d_{5/2}$ bands become distinctive in the heavier ^{127,129,131,133}Cs isotopes. In ^{131}Cs, these bands are populated with nearly equal strengths, despite the fact that the Routhian for band 5 is 170 keV. Similar features have been observed in ^{127,129,133}Cs. The relative energy of the states in the $\pi h_{11/2}$ and $\pi d_{5/2}$ bands in ^{131}Cs allow $I \rightarrow I - 1$, $E1$ transitions. Nevertheless, ^{131}Cs with $Z = 55$, $N = 76$ provides an example of the enhanced octupole correlation that arises from a less pronounced pair of octupole-driving orbits, i.e., $\pi(h_{11/2} \otimes d_{5/2})$ with $\Omega = 1/2$. Wave functions are highly localized for lower components; therefore, the octupole-interaction matrix elements (overlaps) between configurations $h_{11/2}$ and $d_{5/2}$ can be larger for more stable cases with neutron number around $N = 76$.

The $\Delta I = 1$ connecting $E1$ transitions are indeed very weak; furthermore, the intensity determination is marred by the presence of doublets. Spectra of the 140.3, 166.6, and 288.2 keV transitions are relatively clean, and intensity ratios could be determined. Nevertheless, the presence of these $E1$ transitions competing with highly collective $E2$ transitions is already a sign of large $B(E1)$ values. The relative reduced transition probabilities between $\Delta I = 1$, $E1$ and $\Delta I = 2$, $E2$ transitions can be expressed as

$$\frac{B(E1)}{B(E2)} = \frac{1}{1.3 \times 10^6} \frac{E_\gamma^5(E2)}{E_\gamma^3(E1)} \frac{I_\gamma(E1)}{I_\gamma(E2)} \ [\mathrm{fm}^{-2}],$$

where E_γ is in MeV.

The extracted values of the $B(E1)/B(E2)$ ratios for $13/2^+$, $17/2^+$, and $21/2^+$ levels are 1.54×10^{-8}, 2.74×10^{-8}, and 1.34×10^{-8} fm^{-2}, respectively. The $B(E1)/B(E2)$ ratios are similar to those observed in ^{141,143}Cs [21], ^{125}Ba [46], ^{143,145}Ba [47], and ^{117}Xe [48]. Based on the deformation of the even-even core ^{130}Xe [49], the $B(E1)$ values for the ^{131}Cs have been estimated to be around $\sim 6.0 \times 10^{-5}$ W.u., indicating a similar enhancement of octupole correlation in this nucleus.

VI. SUMMARY

The level scheme of the ^{131}Cs nucleus consisting of about 15 band structures has been established up to spin $49/2\hbar$ in the ^{124}Sn (^{11}B, $4n$) reaction using γ-ray spectroscopic techniques with an array of clover detectors. The structures of the various bands have been discussed on the basis of their comparison with the projected deformed Hartree-Fock calculations and the systematics of the nearby nuclei. The low-lying rotational bands based on $\pi g_{7/2}$ (B5), $\pi d_{5/2}$ (B6), and $\pi h_{11/2}$ (B10), evolve into bands B7, B8, and B11, respectively, involving rotationally aligned $(h_{11/2})^2$ quasiparticles. The coupled negative-parity bands B12 and B13 based on three-unpaired-quasiparticle configurations $\pi h_{11/2} \otimes \nu g_{7/2} \otimes \nu d_{3/2}/\nu s_{1/2}$, and the band B14 based on three-quasiproton configurations $\pi(g_{9/2} \otimes d_{5/2} \otimes h_{11/2})/\ \pi(g_{9/2} \otimes g_{7/2} \otimes h_{11/2})$ have also been established. Another striking feature of the present level scheme is the observation of the nearly degenerate dipole bands B2 and B3. These two bands have been assigned high-K three-quasiparticle configurations $\pi h_{11/2} \otimes \nu h_{11/2} \otimes \nu d_{3/2}$. Furthermore, the γ-vibrational bands coupled to the $\pi g_{7/2}$ (B1) and $\pi h_{11/2}$ (B9) one-quasiparticle configurations have also been identified. More investigation is required to identify the structure of band B15. The $E1$ transitions from the $\pi d_{5/2}$ band (B6) to the $\pi h_{11/2}$ band (B9) have been observed in this nucleus, indicating that the corresponding orbitals form an octupole driving pair. The deduced $B(E1)$ values indicate enhancement of octupole correlation in this nucleus similar to that reported for some of the Xe, Cs, and Ba isotopes. The study of electromagnetic properties involving measurement of lifetimes of excited states can throw more light on the intrinsic structures of different bands and their evolution with angular momentum in ^{131}Cs.

ACKNOWLEDGMENTS

The INGA clover array was set up at TIFR Pelletron jointly by TIFR, IUC-DAEF, Kolkata, SINP, Kolkata, and IUAC, New Delhi. The authors would like to thank the collaboration for their cooperation. We gratefully acknowledge the help of all the Pelletron staff for smooth functioning of the accelerator. One of the authors (S.S) is thankful to the Department of Nuclear and Atomic Physics, TIFR, for the laboratory support required for the present work. Financial support from UGC, New Delhi, under the Centre of Advanced Study Funds, CSIR, New Delhi, is duly acknowledged.

[1] I. Ragnarsson, A. Sobiczewski, R. K. Sheline, S. E. Larsson, and B. Nerlo-Pomorska, Nucl. Phys. **A233**, 329 (1974).
[2] Y. S. Chen, S. Frauendorf, and G. A. Leander, Phys. Rev. C **28**, 2437 (1983).
[3] R. F. Casten, and P. von Brentano, Phys. Lett. **B152**, 22 (1985).
[4] L. Hildingsson, C. W. Beausang, D. B. Fossan, R. Ma, E. S. Paul, W. F. Piel, Jr., and N. Xu, Phys. Rev. C **39**, 471 (1989).
[5] E. A. McCutchan, Dennis Bonatsos, N. V. Zamfir, and R. F. Casten, Phys. Rev. C **76**, 024306 (2007).
[6] R. Ma, E. S. Paul, C. W. Beausang, S. Shi, N. Xu, and D. B. Fossan, Phys. Rev. C **36**, 2322 (1987).
[7] K. Hauschild, R. Wadsworth, R. M. Clark, I. M. Hibbert, P. Fallon, A. O. Macchiavelli, D. B. Fossan, H. Schnare, I. Thorslund, P. J. Nolan, A. T. Semple, and L. Walker, Phys. Rev. C **54**, 613 (1996).
[8] S. Frauendorf, Rev. Mod. Phys. **73**, 463 (2001).
[9] H. Hübel, Prog. Part. Nucl. Phys. **54**, 1 (2005).
[10] S. Frauendorf, and J. Meng, Nucl. Phys. **A617**, 131 (1997).
[11] K. Starosta, T. Koike, C. J. Chiara, D. B. Fossan, D. R. LaFosse, A. A. Hecht, C. W. Beausang, M. A. Caprio, J. R. Cooper, R. Krücken, J. R. Novak, N. V. Zamfir, K. E. Zyromski, D. J. Hartley, D. L. Balabanski, Jing-ye Zhang, S. Frauendorf, and V. I. Dimitrov, Phys. Rev. Lett. **86**, 971 (2001).
[12] K. Higashiyama, N. Yoshinaga, and K. Tanabe, Phys. Rev. C **72**, 024315 (2005).
[13] S. Lakshmi, H. C. Jain, P. K. Joshi, I. Mazumdar, R. Palit, A. K. Jain, and S. S. Malik, Nucl. Phys. **A761**, 1 (2005).
[14] S. Kumar, R. Palit, H. C. Jain, I. Mazumdar, P. K. Joshi, S. Roy, A. Y. Deo, Z. Naik, S. S. Malik, and A. K. Jain, Phys. Rev. C **76**, 014306 (2007).
[15] R. Wyss, A. Granderath, R. Bengtsson, P. von Brentano, A. Dewald, A. Gelberg, A. Gizon, J. Gizon, S. Harissopulos, A. Johnson, W. Lieberz, W. Nazarewicz, J. Nyberg, and K. Schiffer, Nucl. Phys. **A505**, 337 (1989).
[16] F. Iachello and A. Arima, *The Interacting Boson Model* (Cambridge University Press, Cambridge, 1987).
[17] R. F. Casten, P. von Brentano, K. Heyde, P. Van Isacker, and J. Jolie, Nucl. Phys. **A439**, 289 (1985).
[18] A. Gelberg, D. Lieberz, P. von Brentano, I. Ragnarsson, P. B. Semmes, and I. Wiedenhover, Nucl. Phys. **A557**, 439c (1993).
[19] O. Vogel, A. Gelberg, R. V. Jolos, and P. von Brentano, Nucl. Phys. **A576**, 109 (1994).
[20] R. Kumar, A. Kumar, S. K. Chamoli, K. Singh, M. Sharma, D. Mehta, N. Singh, S. S. Ghugre, N. S. Pattabiraman, L. Chaturvedi, P. K. Joshi, H. C. Jain, Z. Naik, C. R. Praharaj, and I. M. Govil, Phys. Rev. C **72**, 044319 (2005).
[21] W. Urban, T. Rzaca-Urban, J. L. Durell, W. R. Phillips, A. G. Smith, B. J. Varley, N. Schulz, and I. Ahmad, Phys. Rev. C **69**, 017305 (2004).
[22] M. Sainath, D. Rani Rao, K. Vankataramaniah, and P. C. Sood, Pramana **61**, 1157 (2003).
[23] U. Garg, T. P. Sjoreen, and D. B. Fossan, Phys. Rev. C **19**, 207 (1979).
[24] R. Kumar, K. Singh, D. Mehta, N. Singh, S. S. Malik, E. S. Paul, A. Görgen, S. Chmel, R. P. Singh, and S. Muralithar, Eur. Phys. J. A **24**, 13 (2005).
[25] D. C. Radford, Nucl. Instrum. Methods Phys. Res. A **361**, 306 (1995).
[26] K. S. Krane, R. M. Steffen, and R. M. Wheeler, Nucl. Data Sect. A **11**, 351 (1973).
[27] K. Starosta, T. Morek, Ch. Droste, S. G. Rohozi Imageski, J. Srebrny, A. Wierzchucka, M. Bergström, B. Herskind, E. Melby, T. Czosnyka, and P. J. Napiorkowski, Nucl. Instrum. Methods Phys. Res. A **423**, 16 (1999).
[28] R. Palit, H. C. Jain, P. K. Joshi, S. Nagaraj, B. V. Trao, S. N. Chintalapudi, and S. S. Ghugre, Pramana **54**, 347 (2000).
[29] K. Singh, S. Sihotra, S. S. Malik, J. Goswamy, D. Mehta, N. Singh, R. Kumar, R. P. Singh, S. Muralithar, E. S. Paul, J. A. Sheikh, and C. R. Praharaj, Eur. Phys. J. A **27**, 321 (2005).
[30] K. Singh, Z. Naik, R. Kumar, J. Goswamy, D. Mehta, N. Singh, C. R. Praharaj, E. S. Paul, K. P. Singh, R. P. Singh, S. Muralithar, N. Madhavan, J. J. Das, S. Nath, A. Jhingan, P. Sugathan, and R. K. Bhowmik, Eur. Phys. J. A **25**, 345 (2005).
[31] Y. Liang, R. Ma, E. S. Paul, N. Xu, D. B. Fossan, and R. A. Wyss, Phys. Rev. C **42**, 890 (1990).
[32] L. Hildingsson, W. Klamra, Th. Lindblad, F. Liden, Y. Liang, R. Ma, E. S. Paul, N. Xu, D. B. Fossan, and J. Gascon, Z. Phys. A **340**, 29 (1991).
[33] S. Frauendorf, Nucl. Phys. **A557**, 259c (1993).
[34] S. Frauendorf, Nucl. Phys. **A667**, 115 (2000).
[35] C. R. Praharaj, J. Phys. G **14**, 843 (1988).
[36] Z. Naik, and C. R. Praharaj, Phys. Rev. C **67**, 054318 (2003).
[37] R. E. Peierls and J. Yoccoz, Proc. Phys. Soc. A **70**, 381 (1957).
[38] G. Ripka, in *Advances in Nuclear Physics*, edited by M. Baranger and E. Vogt (Plenum, New York, 1968), Vol. 1, Chap. 3.
[39] R. Bengtsson, and S. Frauendorf, Nucl. Phys. **A327**, 139 (1979).
[40] S. M. Harris, Phys. Rev. **138**, B509 (1965).
[41] S. Sihotra, K. Singh, J. Goswamy, D. Mehta, and N. Singh (in preparation).
[42] Shouyu Wang, Yunzuo Liu, Yingjun Ma, T. Komatsubara, and Yuhu Zhang, Phys. Rev. C **75**, 037302 (2007).
[43] E. Grodner, J. Srebrny, A. A. Pasternak, I. Zalewska, T. Morek, Ch. Droste, J. Mierzejewski, M. Kowalczyk, J. Kownacki, M. Kisielinski, S. G. Rohozinski, T. Koike, K. Starosta, A. Kordyasz, P. J. Napiorkowski, M. Wolinska-Cichocka, E. Ruchowska, W. Plociennik, and J. Perkowski, Phys. Rev. Lett. **97**, 172501 (2006).
[44] A. J. Simons, P. Joshi, D. G. Jenkins, P. M. Raddon, R. Wadsworth, D. B. Fossan, T. Koike, C. Vaman, K. Starosta, E. S. Paul, H. J. Chantler, A. O. Evans, P. Bednarczyk, and D. Curien, J. Phys. G **31**, 541 (2005).
[45] L. Goettig, Ch.Droste, A. Dygo, T. Morek, J. Srebrny, R. Broda, J. Styczen, J. Hattula, H. Helppi, and M. Jaaskelainen, Nucl. Phys. **A357**, 109 (1981).
[46] P. Mason *et al*., Phys. Rev. C **72**, 064315 (2005).
[47] S. J. Zhu *et al*., Phys. Rev. C **60**, 051304(R) (1999).
[48] Z. Liu *et al*., Eur. Phys. J. A **1**, 125 (1998).
[49] S. Raman *et al*., At. Data Nucl. Data Tables **36**, 1 (1987).